Rotating Disk Electrode Design for Concentration Measurements in Flowing Molten Chloride Salts

Kelly M. Sullivan

Thesis submitted to the Faculty of the

Virginia Polytechnic Institute and State University

in partial fulfillment of the requirements for the degree of

Master of Science

in

Nuclear Engineering

Jinsuo Zhang, Chair

Jonathan Link

Alireza Haghighat

June 20, 2022

Blacksburg, Virginia

Keywords: Rotating Disk Electrode, Cyclic Voltammetry, Concentration Measurements, Pyroprocessing, Molten Salt Reactors

Rotating Disk Electrode Design for Concentration Measurements in Flowing Molten Chloride Salts

Kelly M. Sullivan

(ABSTRACT)

Over the past several years as interest in cleaner energy sources has grown nuclear power has come to the forefront. However, as interest in nuclear power grows so does the concern over the amount of high-level radioactive waste produced. Currently, the most popular way to deal with spent nuclear fuel is interim storage until a viable treatment option becomes available. Simply waiting for spent fuel to become safe to handle will take thousands of years and is not a reasonable long-term solution. We will soon run out of space in our spent fuel pools and while more dry storage space can be found it is not an ideal solution. One answer to this problem is the reprocessing of spent nuclear fuel. This could be done with either the plutonium uranium reduction extraction (PUREX) method or the pyroprocessing method. Since PUREX does not have the same level of built-in proliferation resistance as pyroprocessing, pyroprocessing is starting to be seen as a good alternative method. Pyroprocessing would take the spent nuclear fuel from a light water reactor and make it into a metal-based fuel that could be used in certain advanced reactors. Molten salt reactors are of particular interest when it comes to reprocessing spent nuclear fuel because of their unique property of using a liquid fuel. Molten salt reactors and spent fuel reprocessors could be directly connected which would save both time and money as little storage and transportation would need to be considered. Regardless of how and where the used nuclear fuel is being recycled it is important to be able to keep track of the major actinides and fission products in the fuel as it moves through the process. Electrochemical concentration measurements are straightforward and well understood in

static cases when there is only a single element to consider. When additional elements are added, or the system is flowing rather than static, things get slightly more complicated but are still decently well understood. However, in the case of spent fuel reprocessing the system is both be flowing and contains much more than a single element. This case is not well understood and is what this study attempts to understand. Two different rotating electrodes were designed to simulate flowing conditions in an electrochemical cell. The first was a tungsten rotating disk electrode (RDE) and the second was a graphite RDE. We were not able to fully insulate the tungsten RDE and were therefore unable to achieve reliable results. Because of this the tungsten design was put aside in favor of the graphite design, which did prove to be sufficiently insulated. The graphite RDE was tested in two different salt systems: $LiCl - KCl - NiCl_2 - CrCl_2$ and $LiCl - KCl - EuCl_3 - SmCl_3$. In the nickel-chromium system the graphite RDE produced the expected results. The calculated nickel concentration was found to be within 10% of the measured concentration. Calculations of the chromium concentration, however, were not possible due to the deposition of nickel on the graphite surface, which increased the surface area of the working electrode. When the graphite RDE was tested in the second system it was first tested in the ternary salt $LiCl - KCl - EuCl_3$ and was able to produce decent results. The concentration of europium calculated from the scan was within 10% of the measured value. When the RDE was tested in the $LiCl - KCl - EuCl_3 - SmCl_3$ salt the results did not come out as expected. Several rather noisy CV curves were obtained and no alterations to the cell seemed to affect them. At this point it was determined that the reason for the confused scans was a connection problem that could not be remedied within the time frame of this study. While this study does not accomplish the task it set out to do, it is a good step in the direction toward understanding flowing systems containing more than a single element of interest and has successfully designed a reliable graphite RDE.

Rotating Disk Electrode Design for Concentration Measurements in Flowing Molten Chloride Salts

Kelly M. Sullivan

(GENERAL AUDIENCE ABSTRACT)

As interest in nuclear power continues to grow, so does the concern over the amount of high-level nuclear waste produced. More nuclear power means more nuclear reactors and thus more spent nuclear fuel to be dealt with. Currently most used nuclear fuel ends up in interim storage facilities where it is meant to wait until it is safe to handle, which could take several thousand years, or until a reliable disposal method is determined. On this path the amount of spent fuel that requires storage will quickly overrun the amount of storage space safely available. One way to reduce the amount of nuclear waste is to reprocess it to be used as fuel for different types of reactors. The pyroprocessing method takes the spent nuclear fuel from a typical light water reactor and recycles it into fuel that can be used in certain types of advanced reactors, such as molten salt reactors (MSR) and sodium-cooled fast reactors (SFR). The reprocessing system works to separate the usable actinide elements, such as uranium and plutonium, from any fission products or other contaminants. During these processes it is important to be able to keep track of the concentrations of each of these different elements to ensure proper separation. This study examines the use of two rotating disk electrode (RDE) designs that are meant to simulate the flowing conditions found in many reprocessing systems. These RDEs were to be used to measure the concentrations of different elements in molten salt systems. The first design, a tungsten RDE, could not be properly insulated and thus was unable to produce reliable results when tested in the electrochemical cell. The second design was a graphite RDE. This design did prove to be properly insulated

and was able to produce good results when tested in the cell. The graphite RDE was tested in both $LiCl - KCl - NiCl_2 - CrCl_2$ and $LiCl - KCl - EuCl_3 - SmCl_3$. In the first system the concentration of nickel was correctly calculated using the data collected with the graphite RDE, while the chromium concentration could not be due to the nickel deposition on the graphite. In the second system, good results were obtained before the $SmCl_3$ was added to the salt. At this point a connection error became apparent and reliable results were no longer possible. Further study is needed to understand the $LiCl - KCl - EuCl_3 - SmCl_3$ system using the graphite RDE.

Acknowledgments

I would like to thank my advisor, Dr. Jinsuo Zhang, for his mentorship and guidance in my research during the last two years. I would also like to thank Dr. Alireza Haghighat and Dr. Jonathan Link for their guidance on my advisory committee. Finally, I would like to thank all my friends and family who supported me throughout this journey.

Contents

List of Figures

List of Abbreviations

ANL Argonne National Laboratory

BN Boron Nitride

BWR Boiling Water Reactor

CANDU Canada Deuterium Uranium

CV Cyclic Voltammetry

EBR-I Experimental Breeder Reactor I

ICP-MS Inductively Coupled Plasma Mass Spectrometry

LSV Linear Sweep Voltammetry

LWR Light Water Reactor

MSR Molten Salt Reactor

MSRE Molten Salt Reactor Experiment

OCP Open Circuit Potential

ORNL Oak Ridge National Laboratory

PUREX Plutonium Uranium Reduction Extraction

PWR Pressurized Water Reactor

RCE Rotating Cylinder Electrode

RDE Rotating Disk Electrode

RRDE Rotating Ring-Disk Electrode

RRE Rotating Ring Electrode

Chapter 1

Introduction

1.1 Molten Salt Reactors

Research into the use of nuclear power as an energy source began in the US first at Argonne National Laboratory (ANL) in the 1940s. It was in 1951 when a usable quantity of energy was generated by a nuclear reactor for the first time in the US. This was done by the Experimental Breeder Reactor I (EBR-I) designed at ANL [4]. Today the US has a total of 56 nuclear power plants with 93 operating reactors between them. These 93 nuclear reactors have a combined energy generation capacity of 96,555MW. Between the years of 1990 and 2019 these reactors have generated about 20% of the United States total electricity [3]. Worldwide nuclear accounts for around 10% of energy production, coming from around 440 reactors. As of 2020, the USA, China, France, Russia, and South Korea are the top five countries generating the most energy from nuclear power. While France comes in third in terms of TWh, it generates the most energy compared to the size of the country, getting around 70% of its electricity from nuclear power. The USA generates the most energy though this only makes up 20% of the total energy usage. China falls between the USA and France in terms of TWh, but even this large amount only supplies about 5% of their total power [6]. In the US, all of the current operating, energy generating nuclear reactors are Light Water Reactors (LWRs), with about 65% of those being Pressurized Water Reactors (PWRs) and the remaining 35% being Boiling Water Reactors (BWRs). This trend is similar to what

is seen worldwide. The most commonly used type of power reactor is the PWR, followed closely by the BWR. There are currently a few outliers who use slightly different reactor designs. These include heavy water reactors such as the CANDU reactor from Canada, and Gas-Cooled reactors currently in use, primarily within the United Kingdom. Up until the early 2000s there was very little interest in designing and building different types of commercial reactors. The focus, if any, was on expanding the lifetime of the reactors already in use.

Recently there has been renewed interest in expanding and improving the use of nuclear energy throughout the world. Countries and companies are looking to design and build new and improved reactor types, instead of simply expanding the lifetime of existing reactors or building new versions of an old design. Reactors that are more efficient, safer, easier, and cheaper to run. In 2002 the Generation IV International Forum (GIF) selected six types of nuclear reactors that they thought to be the best options for moving forward in nuclear energy technology. One of these reactor types was the Molten Salt Reactor (MSR). The concept of the molten salt reactor was originally conceived as part of the Aircraft Reactor Experiment at Oak Ridge National Laboratory (ORNL) in 1954. This reactor operated for a total of 10 days before it became critical and operated for a further 9.2 days. It operated at a temperature of 880C and used a primary coolant of $NaF-ZrF_4$ (53.09mol% NaF, 40.73mol% ZrF_4, and 6.18mol% UF_4) with the UF_4 and a secondary coolant of sodium-potassium alloy, NaK (77.8wt% K and 22.2wt% Na). This was the first reactor to use circulating molten salt fuel. A few years later, in 1957, ORNL began the Molten Salt Reactor Experiment (MSRE). The MSRE was broken up into two campaigns that culminated into a final breeder reactor design. The first campaign consisted of uranium-235 tetrafluoride dissolved into the $LiF-BeF_2-ZrF_4$ (65mol% LiF, 29.1mol% BeF_2, 5mol% ZrF_4, and 0.9mol% UF_4) molten salt. This salt would flow through a graphite moderator with a secondary coolant of eutectic

lithium-beryllium fluoride, LiFBe (48mol% LiF and 52mol% BeF_2) and would operate at 650C. This campaign had no breeding and was purely proof of concept. The second campaign used uranium-233 instead of uranium-235 and was the first reactor to do so. These two designs then came together in the culmination of the MSRE program. This final design bred uranium-233 from thorium. The primary coolant was $LiF - BeF_2 - ThF_4 - UF_4$ (72mol% LiF, 16mol% BeF_2, 12mol% ThF_4, and 0.4mol% UF_4) flowing through a graphite moderator with the secondary coolant being $NaF - NaBF_4$ (8.1mol% NaF and 92.9mol% $NaBF_4$). The design did work; however, it was ultimately shut down in 1976 due to corrosion and safety issues, including the production of tritium. After the MSRE program was stopped there was very little work put into the development of molten salt reactors. ORNL did look into the feasibility of a denatured molten salt reactor (DMSR) in 1980. This design would be fuel with low-enriched uranium-235 and operate solely as a burner reactor. However, little more was done in regard to the molten salt reactor designs until the 2000s when it was named one of the Generation IV reactors [5].

There are two broad types of MSRs. One uses a liquid fuel dissolved in the primary coolant salt and the second uses solid fuel with a molten fluoride salt primary coolant. Both types of MSRs have significant advantages over the BWRs and PWRs currently used by most. Molten salts boil at much higher temperatures than what is needed for operation, allowing them to be operated at much lower pressures than other types of reactors. Not only does this make reactors easier to house, but it also makes them safer since they will not be producing the potentially explosive levels of steam found in other reactor types. These reactors also offer a higher level of efficiency and generate lower amounts of high-level waste. The liquid fueled MSR has the additional advantages of not using solid fuel and thus has the benefit of not needing to manufacture or dispose of any solid fuel or worry about the possibility of reactor meltdown [1]. One of the more interesting advantages of the molten salt reactor, particularly

the liquid fuel design, is that the fuel salt can be reprocessed through Pyroprocessing to remove any fission products and additional fuel material can be added back to return to the reactor loop. The removal of fission products means that the reactor could potentially have a higher fuel burn-up and less decay heat upon shutdown [5]. With all of the different advantages to MSRs it is clear to see why they were chosen as one of the Gen IV reactors. While the concept and workings of molten salt reactors are well understood, there are still many aspects that need to be better understood before MSRs begin to be commonplace among nuclear reactors. In particular are the fuel reprocessing and Pyroprocessing systems.

1.2 Spent Fuel Reprocessing/Pyroprocessing

As the world's interest in nuclear power grows one of the biggest concerns is waste management. In particular, what to do with the high-level waste produced by the growing number of nuclear power reactors. This is not a simple problem to solve and will certainly not be completely understood or solved for many years. However, there are several options currently being studied that aim to reduce the amount of high-level waste that needs to be handled. One of the more promising waste management options is known as pyroprocessing. The original goal of the pyroprocessing technique is to recycle used nuclear fuel from the currently popular light water reactors into a metallic fuel to be used in metal fueled advanced reactors. Recycling used fuel in this manner allows more energy to be taken from the uranium ore that can then be used to produce electricity [40]. Currently, once the nuclear fuel is no longer usable in the LWRs it is no longer usable anywhere. It is placed in the storage pool until it has cooled down enough to be moved to dry storage where it will need to be isolated for close to 300,000 years before it is safe for further disposal [40]. By using the pyroprocessing technology, most, if not all, of the actinides in the used fuel can be recycled

to be burned in a different reactor. This would reduce the necessary storage time to closer to 300 years, so not only would there be less high-level waste it would also need to be isolated for a drastically shorter period of time [40].

The pyroprocessing method consists of three main steps: the head-end process, the electrochemical processes, and the waste treatment process. The head-end process consists of all procedures that need to be done in order for the used fuel to be in the oxide form necessary for the electrochemical process. For a spent fuel from a light water reactor this would consist of the decladding, voloxidation, and then the oxide feed preparation. Voloxidation is the main process in which the fuel pellet is transitioned into the necessary form. Once the fuel is in the correct oxide form it goes through the electrochemical processes, which consist of electrochemical reduction, electrorefining, and electrowinning. During electrochemical reduction the oxide fuel is reduced to its metal form that is used for electrorefining and many fission products are dissolved into the molten salt bath. The electrorefining process is where the uranium and major actinides are recovered from the fuel. After electrorefining, more uranium and transuranic elements are recovered from the salt bath in the electrowinning process. From there any waste products are disposed of and the uranium and transuranic elements are made into a usable fuel form for the desired advanced reactors [23]. Pyroprocessing was initially designed with its focus solely on LWRs, however, with only slight modifications to the head-end process it can be applied to many other types of fuel from other reactor types [27].

Of course, there are other options for the reprocessing of spent nuclear fuel that would help to eliminate large portions of high-level waste. The best understood of these recycling methods is the PUREX system. This method was developed in the 1950s and used in the US until the 1970s. PUREX and pyroprocessing have essentially the same goal. They both aim to decrease the amount of nuclear waste by reprocessing spent nuclear fuel from nuclear power

reactors. Pyroprocessing has the benefit of having inherent high proliferation resistance due to the fact that it does not separate plutonium from the rest of the actinide elements collected. With PUREX it would be possible to recover pure plutonium from the used fuel, making it a proliferation issue that may be partially avoided by using different methods [27]. Another method that has been considered as a way to, if not decrease the amount of nuclear waste produced, at least postpone the accumulation of high-level waste is called the sourdough method. This method pertains directly to molten salt reactors is. Because molten salt reactors are refueled on-line by adding more fuel salt to what is already present, eventually the volume of salt in the reactor will double. When this point is reached some of that salt can be removed from the reactor and used to start up a second molten salt reactor of the same design. Not only would it drastically increase the lifetime of the fuel salt, but it would also alleviate a large amount of the startup cost for the secondary molten salt reactors [38].

One of the reasons that molten salt reactors have been growing in popularity over the past few years is because of the perceived ease in which spent fuel reprocessing might be connected to these reactors types. Spent nuclear fuel from a light water reactor could be reprocessed into a usable fuel for a molten salt reactor. Building all three of these facilities on the same site could drastically reduce storage and transportation costs while also reducing the level of waste produced [22]. Because of the liquid nature of the molten salt reactor's fuel, it is even possible to have the reprocessing unit directly connected to the reactor [8, 14, 35, 36]. Another type of molten salt reactor, the non-moderated thorium molten salt reactor (TMSR-NM), is specifically designed to use the spent fuel from PWRs as its startup fuel. From the first TMSR the fuel can then be used to start up a second generation of the same reactor [10]. The ways in which spent fuel reprocessing and molten salt reactors can be connected are still in the early stages of study, but it is clear that a partnership between the two would

be highly beneficial in terms of reducing the amount of high-level nuclear waste.

Regardless of which type of spent fuel reprocessing method is chosen it is extremely important to be able to keep an accurate track of the amount of each element within the system. With pyroprocessing and PUREX it is important to know the exact concentrations of the major actinides in the spent fuel throughout the entire process to ensure the necessary proliferation requirements are being met and that the solution is replaced and replenished at the appropriate points in order for it to continue to run correctly. Measuring the concentrations of a single element in a molten salt solution electrochemically is a fairly straightforward process. Assuming the peak current of the element of interest is known in the particular solution the concentration of that element in the solution can easily be calculated. To determine the peak current of the element of interest in a static system one needs only to create the appropriate electrochemical cell and run a CV scan in the desired potential range. This becomes slightly more difficult when there is more than a single element's concentration to measure, or the system is no longer static. While these two cases are less straightforward than the simplest case they are still fairly well understood. However, in the case concentration measurements during spent fuel reprocessing the system is both flowing and there is far more than a single element to keep track of. In this case, electrochemical concentration measurements are not well understood. This is the case that this study attempts to understand further through the use of a rotating disk electrode.

1.3 Literature Review

1.3.1 Rotating Electrodes Designs and Uses

During pyroprocessing and other fuel reprocessing methods it is important to be able to keep track of the concentrations of the different elements found in the fuel. This can be done electrochemically by the use of a three-electrode cell system. Most studies regarding the concentration measurements in spent nuclear fuel have been done under static conditions. The working, counter, and reference electrodes would be placed in a molten salt sample and a cyclic voltammetry would be run using a potentiostat. The peak current, designated by the reduction and oxidation peaks, would then be used to measure the concentration of the element of interest. While this method is fairly accurate, it is not suitable or efficient for real world applications. During the Pyroprocessing process the molten salt will be flowing through the system as the elements are separated for increasing efficiency. Because of this it would be more realistic and efficient to be able to measure the concentrations of elements in a flowing system. This can be fairly well simulated through the use of a rotating electrode. A rotating electrode would cause the molten salt in the system to flow similar to how the molten salt solution in the Pyroprocessing system would flow past a working electrode. These measurements can be taken in the same way as would be done in a static system, with the only difference being the shape of the final CV curve and the equation used to calculate the concentration. Instead of peak current peaks, one would have limiting current plateaus. These rotating electrodes have been shown to work well in many low temperature, aqueous systems. However, their use in higher temperature, molten salt systems has been limited. Even more limited is their use in measuring the concentrations of more than one element in a system at a time. Most of the tests that have been done with rotating electrodes in bulk salts had only one element of interest. This again is not realistic, as in the typical system

there will be many different elements that need to be kept track of and it would be nearly impossible to focus on only one element at a time.

There are four basic types of rotating electrodes that are generally used in electrochemical studies. They are the rotating disk electrode (RDE), the rotating cylinder electrode (RCE), rotating ring electrode (RRE), and the rotating ring-disk electrode (RRDE). The RDE generally consists of an electrode material that has been insulated so that only a disk of electrode will be in contact with the system. The RRE generally consists of a tube-shaped electrode material that is then insulated both on the inside and the outside so that only a ring of electrode is in contact with the system at any given time. As may be assumed given the name, the RRDE is a combination of both the RDE and the RRE. The electrode material is insulated such that a ring and a disk of material are all that is exposed to the system, the ring and the disk being separated by insulating material. The RCE is generally a little less defined than the previous rotating electrodes. An RCE may be designed similarly to an RDE or an RRE, in that a rod of electrode material is sheathed in insulating material so that only a known amount of the rod, or cylinder, is exposed to the system. In most instances, however, a simple rod of electrode material that has been attached to a rotator, with no additional insulation or modifications, has been referred to as an RCE. While they are all relatively similar designs, each type of electrode requires the use slightly different techniques in order to evaluate their data. And each has their own pros and cons depending on the application they are being used for. However they are fabricated, each of these four basic rotating electrode designs have been used in electrochemical studies of molten salt systems.

Perhaps one of the simplest rotating electrodes to fabricate is the RCE. At its most basic the RCE electrode consists of only a rod of electrode material, with no additional insulation, which is then attached to a rotator. A rotating electrode of this type may also consist of some electrode material that has been insulated such that only a certain known amount of

material is in contact with the system. Before being adapted for use in higher temperature systems, such as molten salts, RCEs were used for electrochemical measurements in many lower temperature systems in both its simpler and its more complex design [11, 16, 17, 29]. RCEs are generally used for studies that require turbulent flow. Most often they are seen in electrodeposition, cementation, and corrosion and dissolution studies [29]. Rappleye et al. opted for a simple tungsten rod attached to a rotator, with no additional insulation [34]. This design is easily the simplest to fabricate and use. Unlike the RDE and RRDE, this type does not require precision fabrication, other than ensuring that the electrode rod is level, or proper placement within the system. Rappleye used an RCE of this type to measure the exchange current density and mass transfer coefficient in a LiCl-KCl molten salt system. While this design has the benefit of being easy to fabricate it did prove to have several major drawbacks. The tungsten rod could not be rotated at any rate higher than 500rpm before it would start to vibrate. Such a low rotation rate would not allow for clear limiting current plateaus to be observed making calculations difficult. Additionally, the lack of additional insulation on the working electrode made it difficult to measure the RCEs working surface area. The height of the working electrode was taken from the immersion depth, which was found by observing the salt that had adhered to the RCE after removal from the system [34]. This height was then used to determine the working electrode surface area and was not reliable. The combination of these two limitations to this RCE design make it a poor choice for more precise electrochemical measurements in molten salt systems.

Two less common rotating electrode designs are the RRDE and RRE. These two designs are markedly more complicated to fabricate than the RCE described above, though they do have their benefits. Using a RRDE it is possible to obtain certain information that would be available with stationary electrodes but is not possible with RDEs or RCEs [2]. RRDEs are most often used in collection and shielding experiments. In collection experiments the disk

generated species can be observed and studied at the ring. In shielding experiments, the flow of the bulk electroactive species to the ring is perturbed because of the disk [2]. RREs can be used on their own and while the theoretical treatment of RREs is more complicated than that of an RDE or RRDE they do have the benefit of having larger mass transfer than would be seen with an RDE or RRDE [2]. As with the RCE, the RRDEs and RREs were originally designed for use in low temperature, aqueous systems [13, 25]. Phillips et al. later adapted the RRDE to be used in low temperature, aqueous, and higher temperature molten salt studies. Their design consisted of a ring and disk of glassy carbon insulated by Pyrex and Teflon [24]. This electrode was tested in both an aqueous and higher temperature systems. The RRDE worked as expected at both room temperature and at 175C. However, at higher temperatures, 450C, the Teflon insulation was damaged. This design was stable at rotation rates up to 6000rpm [24] and provided a different insulation type would be a decent choice for a rotating electrode in certain molten salt electrochemical experiments. One does need to be cautious when choosing an RRE or RRDE as the multiple electrode-insulator interfaces increase the possibility of not achieving a tight seal and allowing the solution to seep between the insulation and electrode material.

The most popular and well understood choice of rotating electrode in molten salt studies is the RDE [16, 29]. This type is much more complicated to fabricate then a basic RCE but slightly easier than a RRDE or RRE. When fabricating an RRDE or RRE one needs to be careful to achieve a tight seal between the electrode material and insulation material on two or three surfaces. With the RDE one only needs to be concerned with a single interface. A typical RDE consists of a rod of electrode material that has been insulated in such a way that allows for only a disk of electrode material to be in contact with the system at any given moment. Ge et al. used this type of rotating electrode in their study of Eu(III) and Eu(II) in LiCl-KCl. Their RDE consisted of a rod of graphite insulated in a boron nitride

tube, using the difference between the thermal expansion coefficients of graphite and boron nitride to achieve a sufficient seal between the two [18]. A similar method was employed by Ramaswami and Selman using gold as the electrode material and alumina as the insulating material in their study of molten carbonates [33]. The graphite design by Ge was stable at rotation rates up to at least 2400rpm and temperatures of at least 773K [18]. The rotation rates used in Ramaswami's experiments were not stated so it is unclear how stable the design might be at higher speeds. Ramaswami and Selman noted in their two papers that there was significant evidence of a leak between the gold electrode and the alumina insulation [32]. This could be caused by the fact that the pure gold used in the RDE becomes soft at temperatures over 650C leading to an unreliable seal. This problem was not seen in Ge's graphite RDE design indicating it might be a more reliable choice for a rotating electrode in high temperature systems. Another design for an RDE was fabricated by Copham and Fray in their study of the electrolysis of molten zinc chloride electrolytes [9]. This design consisted of two disk plates that were rotated about a central pivot point. The purpose of this design was to show that by using rotating electrodes one can place the electrodes closer together than can be done with stationary electrodes while still retaining a high current efficiency in electrowinning cells. This concept was successfully shown with this RDE design and with a sloped version of the same design. However, this design was only stable up to about 200rpm before the efficiency would drop drastically, most likely caused by the increasing downflow of the electrolyte between the two disks [9]. One additional RDE design to be considered would be the detachable disk electrode designed by Liu et al. This design consists of a disk of electrode material placed inside of a boron nitride nut and sealed in place with a stainless-steel fastener. A small hole at the bottom of the nut allows for a small portion of the electrode material to be in contact with the salt [28]. When this design was tested it was found that there was likely not an adequate seal between the electrode and insulation thus allowing the electrode surface area to grow over time indicating that it is not suitable

for more precise electrochemical analysis. It appears that Ge and Ramaswami achieved the most promising design for analytical electrochemistry studies, given one chooses appropriate material.

There are many different types of rotating electrodes and each one has its own benefits and drawbacks depending on the application it is used for. The most complicated to fabricate is the RRDE and RRE making erroneous calculations more probable. However, they can be used for certain types of experiments that others cannot. At its simplest the RCE is the easiest to fabricate but has the largest chance for calculation errors. The RDE is a solid middle ground option for precise electrochemical measurements. With the right material selection this type of rotating electrode can be relatively simple to fabricate and has the most diversity of application and design.

1.3.2 CVs for Concentration Measurements

Cyclic voltammetry (CV) is a commonly used technique in electrochemical studies. CV scans are completed by running through a set range of applied potentials and recording the current at each step, first in one direction and then repeating the process in the opposite direction. The applied potential during the CV scan is varied linearly with respect to time, set by the scan rate. The voltammograms produced during a CV scan show a plot of applied potential versus current. A CV scan is generally completed using a three-electrode setup: a working electrode, a counter electrode, and a reference electrode. The potential range applied is determined based on the material of the working electrode and the analyte. CV voltammograms can be described by the Nernst Equation (1.1), which compares the potential of the cell to the standard potential of the element of interest and the activities of the reduced and oxidized analyte when the system is at equilibrium. Though, more often

the standard potential is often replaced by the formal potential, and the activities replaced by their corresponding concentrations.

$$E = E^{0'} + \frac{RT}{nF} ln \left(\frac{C_O}{C_R} \right) \tag{1.1}$$

Here $E^{0'}$ is the formal or apparent potential, R is the universal gas constant, T is the temperature, n is the number of electrons, F is the Faraday constant, and C_O and C_R are the concentrations of the oxidant and reductant respectively. As the potential is scanned in the negative direction the species is being reduced. At the cathodic peak potential, the species at the electrode surface has been completely reduced, showing the peak cathodic current. This reduction peak current can be used to measure the concentration of the reactant. When the potential switches to scan in the positive direction, the species is being oxidized. Similar to the reduction, the species at the electrode surface is completely oxidized at the anodic peak potential, showing the peak anodic current. This oxidation peak current can then be used to calculate the concentration of the product.

CV scans are most commonly seen using static electrodes with no movement or stirring of the solution. In this case the scan generally displays two peaks, one negative and one positive. These peaks represent the oxidation and reduction of the analyte. In this type of system, the peak current can be found by applying the Randles-Sevcik equation [12], for soluble-soluble reactions,

$$i_p = 0.446 nFAC^0 \left(\frac{nFvD_o}{RT} \right)^{1/2} \tag{1.2}$$

where i_p is the peak current, A is the electrode area, v is the scan rate, and D_O is the diffusion coefficient. For soluble-insoluble reactions one would apply the Berzins-Delahay

equation [41],

$$i_p = 0.611nFAC^0 \left(\frac{nFvD_o}{RT}\right)^{1/2} \tag{1.3}$$

While slightly less common, CV scans can also be taken using rotating electrodes or in flowing systems. In this case the CV no longer produces a reduction and oxidation peak but rather plateaus. The difference in shape is due to the different ways in which the analyte is moved toward the working electrode, by convection, migration, or diffusion. In a static system, with stationary electrodes, the only mode of mass transport is diffusion arising from the difference in concentrations in the bulk salt and at the electrode. With rotating electrodes, however, the analyte is transported toward the electrode by both diffusion and convection. Determining the limiting currents in this case is slightly more complicated than the static case and is dependent on the geometry of the rotating electrode. For a RDE, the Levich equation is used to find the limiting current,

$$i_{D,l} = 0.62nFAD_o^{2/3}\omega^{1/2}\upsilon^{-1/6}C_o \tag{1.4}$$

where ω is the rotation rate and υ is the solution viscosity [2]. For an RRE you have different equation with which to solve for the limiting current,

$$i_{R,l} = 0.62nF\pi\left(r_3^3 - r_2^3\right)^{2/3} D_o^{2/3}\omega^{1/2}\upsilon^{-1/6}C_o \tag{1.5}$$

where r_2 and r_3 are the inner and outer diameter of the ring of the electrode [2]. And for the RCE you have yet another equation for finding the limiting current of the analyte,

$$i_{C,l} = 0.0791 z F C_b U^{0.7} \left(\frac{R_1}{\upsilon}\right)^{-0.3} \left(\frac{\upsilon}{D}\right)^{-0.644} \tag{1.6}$$

where zF is the Faradaic equivalence [15]. Each of the different equations are derived using the steady-state convection diffusion equation, with the differences arising from the different velocity profiles due to their differing geometries.

CV scans accompanied with the appropriate limiting or peak current equation can then be used to determine the diffusion coefficient or concentration of the analyte, deepening on what information is already known. CV is a very important method for concentration measurements in both aqueous and molten salt systems. Given a system with only a single analyte, under static conditions, determining the concentration of the analyte from a CV scan is a relatively simple process, assuming the diffusion coefficient is known [20, 21, 39, 41]. One simply runs a scan in the correct potential range, determines the peak current and utilizes the Randles-Sevcik or Berzins-Delahay equation. The same can be said for a rotating system with a single analyte [13, 18, 24]. One determines the limiting current from the plateau in the CV curve and then utilizes the appropriate equation. Concentration measurements using the CV scans become slightly more difficult and less reliable when the systems have more than one analyte. In a static system with more than one analyte the first reduction peak often causes a convolution in the second and the second would then disrupt the peak of the third and continue on in this manner depending on the number of reductions and oxidations present in the solution. The baseline of the second or third reduction or oxidation peak would be distorted by the tail of the previous peak, thus distorting the height of the following peaks, and providing an inaccurate peak current. Work has been done to eliminate this issue by taking either the partial derivative or the partial integral of the CV current data with respect to the potential [37]. Doing this would isolate each individual reduction and oxidation peak and allow for more accurate concentration calculations. While this method works well on

CVs taken with static systems it has yet to be applied to rotating or flowing systems. In fact, very little work has been done with flowing molten salt systems containing more than a single element. With so little work done on the topic it is difficult to tell whether or not the same distortion that is seen in the static systems would be seen in the flowing system. From the work of Rappleye and Simpson, it appears as though a similar issue does in fact arise [34]. If this is the case, it is unclear as to whether or not the same method used to analyze a static CV would work for a CV in a flowing system.

Chapter 2

RDE Design

Rotating electrodes are incredibly useful for simulating flow during electrochemical tests. They have been used extensively in aqueous and other low temperature systems. However, they have found relatively little use in the higher temperature molten salt systems. This is likely due to the difficulty in designing a sufficiently insulated rotating electrode, be it a disk, cylinder, or ring-disk. Not only must the insulator material be capable of withstanding the high temperatures found in molten salt systems, but it must also be able to survive the molten salt's corrosive nature. Once a suitable material has been determined it is important to be able to create a sufficiently tight seal between the insulator and the electrode material such that the molten salt does not seep in between the two. This will often also factor into the choice of insulating material. Ensuring a tight seal around the electrode material is perhaps the most challenging aspect of designing a rotating electrode for electrochemical tests. There have been many attempts at designing a reliable rotating electrode, though many of them are either complicated to reproduce or costly. Here two different potential RDE designs to be used in molten salts systems are examined. These designs are meant to be easy to reproduce and more cost effective. A rotating disk electrode was chosen due to the simplicity of its design. Initially tungsten was chosen as the electrode material due to its capability to act as an inert electrode and thus the wide range of applications. The second design uses graphite as the electrode since it leads to a much simpler design concept.

2.1 Tungsten RDE

The general concept for the design of a tungsten RDE is simple. A rod of tungsten must be insulated so that only a small disk of material is exposed. The RDE must then be somehow attached to the shaft of a motor meant to rotate the electrode at the desired speeds. The most important and difficult part of the design is ensuring that there is a tight seal between the electrode material and the insulating material. Since tungsten has a very low thermal expansion coefficient it was not possible to take advantage of the difference between the expansions of the electrode and insulating material to provide a tight seal, as has been done in other designs. Another method of securely insulating the tungsten had to be determined. Another difficulty in designing a tungsten RDE was the extreme difficulty in modifying the tungsten in any way. Tungsten is very hard and thus very difficult to cut into different shapes and sizes. This adds the additional question of how to attach the RDE to the rotator shaft since the tungsten itself could not be modified to connect to the shaft. Several different designs and alterations were considered in attempts of coming up with solutions to these two problems in hopes allowing for the creation of a reliable tungsten RDE.

The solution for how the tungsten RDE would be attached to the rotator shaft was fairly simple. The tungsten would be attached to a secondary piece of conductive material that could be modified to attach to the rotator shaft via screw connection. Initially the secondary piece of conductive material was chosen to be stainless steel. Easy enough to modify as desired but hard enough that it would not break. However, the stainless steel was eventually determined to be too heavy to be used. This was thought to cause the electrode to wobble a great deal during rotation. The wobbling would cause a turbulent flow when a laminar flow was desired, along with a great deal of noise in any electrochemical scans taken with the RDE. So, the stainless steel was then switched out for a graphite base, which was much lighter and easier to fabricate. The graphite, and previously the stainless steel, was modified

Figure 2.1: Graphite-Tungsten Connection

such that one end had the same diameter as the tungsten while the other end had a much larger diameter. The base end of the graphite was to have a large enough diameter so that there was room for a screw connection to attach it to the end of the rotator shaft. With the graphite base designed as such, it would then be attached to the tungsten piece using a spring. While a stainless-steel spring was initially chosen as the connection mechanism, it was ultimately switched to a copper spring. This was due to the fact that the stainless-steel spring had been seen to corrode during use in the electrochemical test. A copper spring was much more resistant to this corrosion. This design, shown in Figure 2.1, would be the main electrode component of the RDE. With the connection between the two secured, the tungsten and graphite would need to be insulated to prevent the molten salt from coming into contact with anything other than the desired disk of tungsten.

For the first iteration of the tungsten RDE alumina was chosen as the insulating material. Alumina was chosen because of its stability at high temperatures and in highly corrosive environments. The tungsten and the head of the graphite were placed inside of an alumina tube with the base of the graphite meeting end of the tube and then cemented in place using

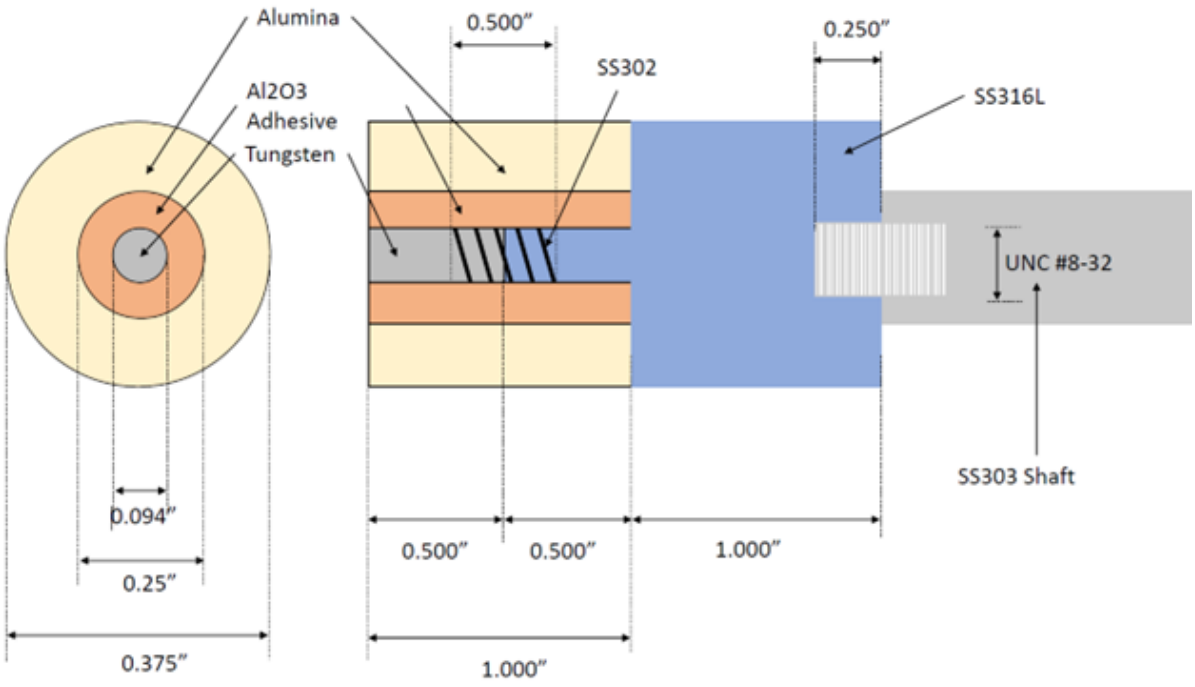

Figure 2.2: Tungsten RDE Design 1

an alumina adhesive. This design is shown in Figure 2.2. After the adhesive had been allowed to cure, the RDE was tested on the rotator motor. This test showed significant wobbling in the RDEs rotation, which was ultimately caused by the electrode being off center from the alumina tube. After several attempts to find methods to ensure proper alignment between the graphite and alumina, it was determined that alteration to the design was needed.

This alteration came in the form of a new insulation material, boron nitride. With this alteration the inner diameter of the boron nitride tube matched the diameter of the graphite base so that the tube would be able to encompass the entire RDE. Having the two diameters match made sure that the graphite, and thus the tungsten, were perfectly centered in the insulation. A boron nitride tube was chosen to replace the alumina tube due to its low thermal expansion coefficient. When heated the graphite's greater thermal expansion coefficient would cause a tight seal between the boron nitride and the graphite base of the electrode.

Figure 2.3: Boron Nitride Coated Tungsten RDE

The alumina adhesive used in the previous iteration of this design was then be used to fill in the remaining space between the tungsten and the boron nitride tube. While this new design did in fact eliminate the wobbling seen previously, it was ultimately found that it did not completely insulate the tungsten and graphite from the molten salt. The alumina adhesive was found to dry porous and allowed the salt to seep through and interact with the tungsten, graphite, and copper spring. Several different adhesive types were tested in place of the alumina, and all presented the same issue. They were too porous to provide sufficient insulation. To combat this problem a boron nitride aerosol coating was used [19]. The coating was meant to act as a sealant at the head of the RDE. Any pores or gaps in the adhesive would be sealed by the boron nitride spray, preventing any salt from seeping through, as shown in Figure 2.3. Unfortunately, the boron nitride aerosol on the adhesive did not successfully insulate the RDE. To combat this the graphite, copper spring, and tungsten rod were all coated in the BN spray before being cemented into the boron nitride tube. The hope was that even if the salt did manage to get through the adhesive and outer layer of boron nitride this inner coating would protect the graphite and copper from the salt.

Even with this addition it was found that the salt was still finding its way through the insulation to interact with the graphite and a copper spring. In an attempt to eliminate this possibility completely the design was modified once again. The tungsten rod was made longer so that the graphite/tungsten connection might be insulated separately from the tungsten. The tungsten was insulated with a small diameter alumina tube and alumina adhesive and then coated with the boron nitride spray. The graphite, copper spring, and tungsten connection was then insulated in the same manner as the preceding design, with the boron nitride tube and alumina adhesive. There was a small gap between the alumina tube and the boron nitride tube that was insulated using the boron nitride spray. The RDE would then be inserted into the salt so that it only came part way up the alumina tube. This was meant to prevent the possibility of the salt ever making its way to the graphite and copper wire. This design was significantly more difficult to fabricate and did not produce any better results than the previous, so it was determined that earlier design was the most promising option for a tungsten RDE, though it does still require a few modifications.

2.2 Graphite RDE

The concept for the graphite came from a paper by Ge, et al., "In Situ Electrochemical Study of the Coexistence of Eu^{3+} and Eu^{2+} in Molten LiCl-KCl by Rotating Disc Electrode" [18]. Here, Ge designed a simple graphite RDE. Unlike with the tungsten RDE, the graphite design does not require a secondary insulator in the form of an adhesive. This RDE takes advantage of the difference between the thermal expansion coefficient of the insulating material and the electrode material. The idea is that the graphite's larger thermal expansion coefficient will cause the graphite to seal itself into the insulator, thus preventing any salt from seeping past the exposed graphite disc. The insulating material for this design is a boron nitride

tube, chosen for its high thermal stability, poor wetting properties in the molten salt, and relatively small coefficient of thermal expansion. Ge demonstrated that RDE works well in molten chloride salts, and, unlike many previous designs by others, works well at high rotation rates, making it a good choice for simulating flow conditions during electrochemical tests [9, 34]. While it did work well, it also had a few drawbacks that needed to be addressed before being used in further studies.

One feature that made this design less than ideal was the large surface area of the disk of the electrode. As the RDE would serve the working electrode in any electrochemical tests, it is generally desired that the working surface area be much smaller than that of the counter and reference electrodes' surface areas. The large size of Ge's RDE made this more difficult to achieve than necessary. In this work, that particular drawback was easily altered by using a similar design to that used in the graphite portion of the tungsten RDE. Since the RDE still had to be able to attach via the screw connection to the rotator shaft the base of the electrode could not decrease much in diameter. To accommodate this the graphite was modified such that a certain length had the desired electrode diameter while the remaining length had a diameter large enough to house the screw connection. The boron nitride tube would then have the same inner diameter as the diameter of the smaller end of the graphite and a matching outer diameter with the larger end of the graphite. Once the boron nitride tube and graphite were cut to the desired length and diameter, the smaller graphite end was inserted into the boron nitride tube. The base end of the graphite would sit directly centered at the end of the tube. When heated the graphite would expand and seal itself into the insulator preventing any salt seepage. While this design is considerably simpler than the tungsten RDE design, the size of the graphite diameter and boron nitride inner diameter are very important. If the graphite is even slightly too small in comparison to boron nitride tube, there will not be a reliable seal between the two. Without this seal the salt would seep

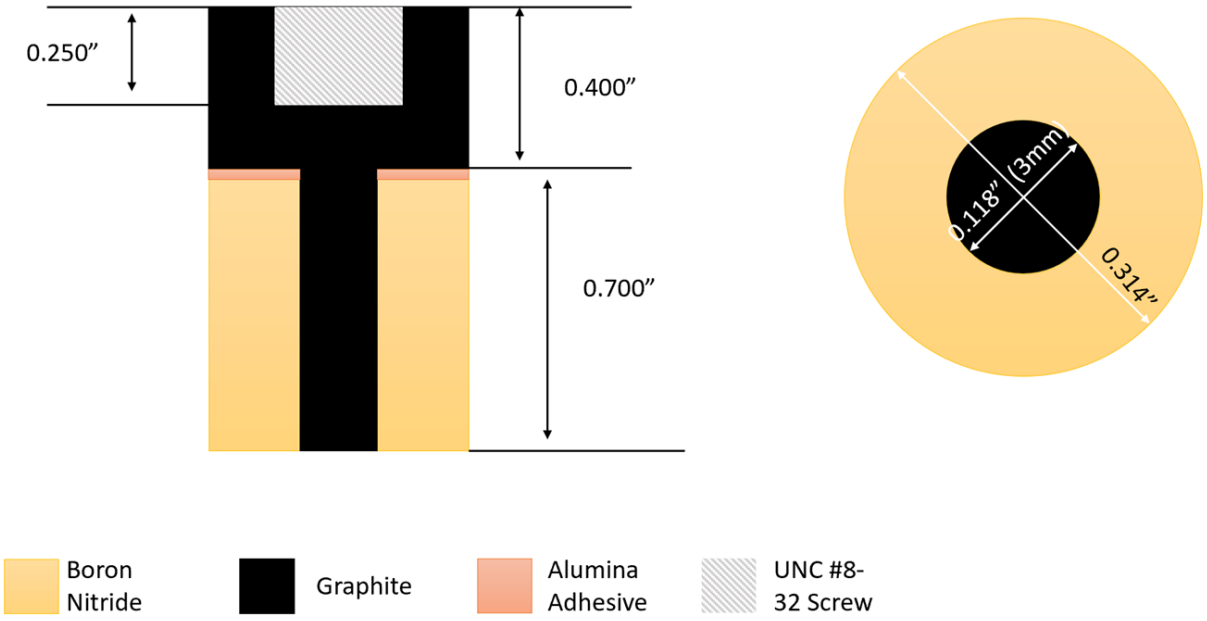

Figure 2.4: Graphite RDE Design

up the shaft of the graphite causing undesired reactions on the working electrode related to surface area size. Clean and reproducible tests would not be possible. The exposed graphite base would be coated in a boron nitride aerosol that would prevent any accidental contact with the salt system when placing the RDE.

The second modification made to this design was to add a small amount of adhesive between the graphite base and the end of the boron nitride tube. When heated the graphite and boron nitride are tightly sealed together and cannot be separated. However, when at room temperature the two can easily be taken apart. While this does have some benefits in regard to cleaning the electrode, it does make it difficult to handle the RDE before it is at temperature. To alleviate this difficulty, a small amount of alumina adhesive was added between the end of the boron nitride tube and the graphite base. Once cured, this would prevent the insulator from sliding down or off the electrode material when at room temperature.

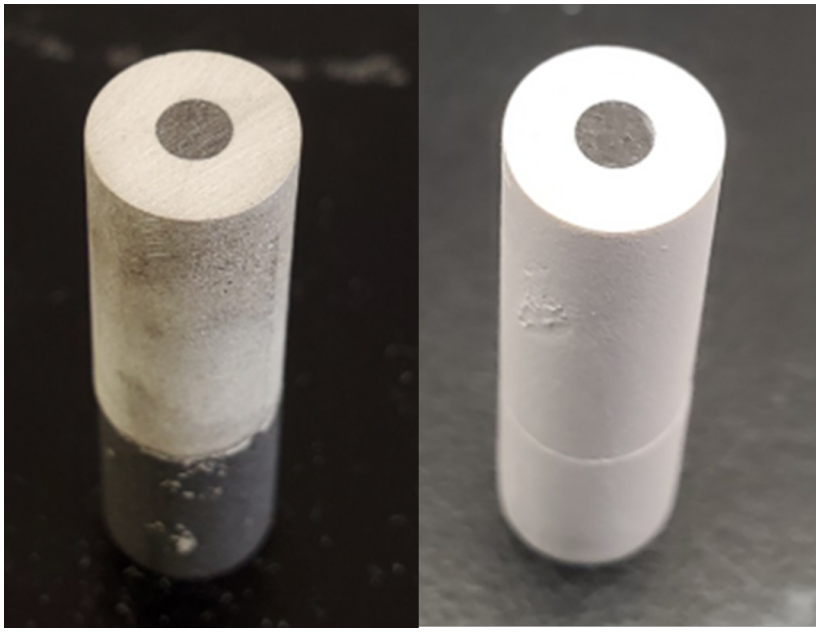

Figure 2.5: Graphite RDE without and with BN coating

Chapter 3

Experimental Material and Methods

3.1 Tungsten RDE

A tungsten RDE was designed to simulate flowing conditions during electrochemical tests in molten salt systems. The first design consisted of a small piece of tungsten connected to a piece of graphite via stainless-steel spring. The tungsten/graphite electrode was then cemented into an alumina tube in order to insulate all but a disk of the tungsten from the salt system. The electrode would be attached to a stainless-steel shaft via a screw connection, which in turn was mounted into a motor that would rotate the RDE at the desired rates. Before the tungsten RDE was used in the molten salt system it was tested on the rotator to ensure a smooth rotation. There must be a smooth rotation to allow for the necessary laminar flow during the electrochemical tests. A wobbly or erratic rotation would cause a turbulent flow or severe noise in the system. The RDE was attached to the motor and rotated at steadily increasing rotation rates and watched for any visible wobbling or an off-center rotation. The first tungsten RDE design did not show a smooth rotation at high rotation rates, so it was altered. The second iteration of the tungsten RDE was tested in the same way as the first on the rotator. With this new design smooth, even rotations were observed at the desired rotation rates.

With the tungsten RDE displaying a steady rotation, it could then be used for concentration measurements in the molten salt system. The RDE was to be used to measure the

concentration of lanthanum in a molten chloride salt system. The salt system consisted of LiCl (ASC Reagent, >99%, Sigma-Aldrich), KCl (Ultra Dry, >99.99%, Alfa Aesar), and $LaCl_3$ (99.99%, APL Engineering). The bulk salt, 22.5352g LiCl and 27.5588g KCl, was well mixed and placed in an alumina crucible and heated first to 300C and held for 8hrs before then increase in temperature to 450C, the operating temperature, to remove any moisture or impurities. The electrochemical cell consisted of a three-electrode system immersed in the molten salt. The tungsten RDE was to act as the working electrode. The counter electrode was graphite, and the reference electrode was Ag/AgCl housed in an NMR tube. The Ag/AgCl reference consisted of 0.1677g KCl, 0.1405g LiCl, and 0.0034g AgCl (99.999%, Sigma-Aldrich) that had been well mixed before being placed in the NMR tube. A silver wire was then placed in the reference electrode housing. The electrodes were immersed in the LiCl-KCl bulk salt with 0.5165g $LaCl_3$, one weight percent of the bulk salt, and the system was allowed to come to equilibrium. The RDE was tested first with zero rotation to verify its functionality. Once the system had reached its equilibrium OCP and CV scans were run using a Gamry potentiostat 600+. After each series of tests, the tungsten RDE was modified in attempts to eliminate any issues that arose during the electrochemical tests, and the tests were run again. All tests were run in a controlled argon atmosphere glovebox.

3.2 Graphite RDE

3.2.1 $LiCl - KCl - NiCl_2 - CrCl_2$

Two experiments were run with the graphite RDE design. The first experiment was run using LiCl (ASC Reagent, >99%, Sigma-Aldrich), KCl (Ultra Dry, >99.99%, Alfa Aesar), $NiCl_2$ (Anhydrous, powder,99.99%, Sigma-Aldrich), and $CrCl_2$ (Anhydrous, powder,

99.99%, Sigma-Aldrich). Nickel and chromium were chosen as the two analytes for this experiment for several reasons. First, they were selected because of the relative positions of their oxidation and reduction potentials. Both potentials are located far enough away from each other and those of potassium and chlorine to ensure clear visibility of their respective oxidation and reduction. The second reason was that they did not have any reaction with any of the other materials in the system at the operating temperature. To begin, 22.4304g of LiCl and 27.5194g of KCl were thoroughly mixed and placed in an alumina crucible. The bulk salt was then heated to 300C and held for eight hours to remove any oxygen or other impurities. The temperature was then increased to the operating temperature of 450C and allowed to come to equilibrium. Once the LiCl-KCl has melted and stabilized, the electrochemical tests were started. The electrochemical tests were done using a three-electrode setup. The graphite RDE served as the working electrode, the counter electrode was a tungsten rod, and the reference was Ag/AgCl consisting of LiCl-KCl-1wt%AgCl housed in an NMR tube with a silver wire. The RDE was connected to the rotator via a stainless-steel shaft. Before any additional analytes were added to the bulk salt several tests were run using just the blank salt. OCP and CV curves were run both under static conditions, with no rotation of the RDE, and with the RDE rotating at various speeds. The RDE was tested at 1000rpm, 1500rpm, 1800rpm, 2000rpm, 2200rpm, and 2400rpm. Doing this had the benefits of showing if the RDE was working as expected and if there were any significant amounts of impurities in the salt. First the three electrodes were immersed in the salt and the system was allowed to come to equilibrium. With the electrodes inserted in the salt an OCP test was run to ensure that the system had indeed come to equilibrium before further tests were done. Once the system was verified as stable a CV scan was run ranging from -2.5V to 1V, between the reduction potentials of potassium and chlorine. The CV scan was run for 6 cycles. After the CV scan had finished the RDE was electrochemically cleaned, and the testing process was started again. This process was done with zero rotation of the RDE and

at each of the selected rotation rates. Salt samples were taken before and after the CV tests to be used in ICP-MS analysis to test for any impurities in the salt that might affect the concentration measurements that would be done. As with the tungsten RDE, all tests were carried out in a controlled argon atmosphere glovebox.

Once RDE had been confirmed to work in the blank bulk salt it was tested in the tertiary salt, $LiCl - KCl - 1wt\%NiCl_2$. With the bulk salt already at operating temperature, one weight percent, 0.5311g, of $NiCl_2$ was added to the LiCl-KCl in the alumina crucible. Before tests were started a salt sample was taken to be used in running an ICP-MS test to verify the concentration of the nickel in the salt. The three electrodes were then inserted into the salt, after being cleaned from the previous tests, and the system was allowed to regain an equilibrium. An OCP scan was run while the system was equilibrating. Once the OCP scan showed that the system had stabilized a CV scan was run. The first sets of OCPs and CVs the tests were completed with zero rotation of the RDE. These static scans would be used to compare to the flowing scan taken with the rotating RDE. After the static scans were completed the RDE motor was turned on and the RDE was set to rotate at the desired rates. To start CV scans were run with the RDE rotating at 1000rpm, 1500rpm, and 2000rpm with varying scan rates. These scans quickly made it clear that a CV scan would not provide the data required for concentration measurements due to the convolutions caused by the back scan. Because of this, it was decided that Linear Sweep Voltammetry (LSV) was better suited to obtain the desired data from the RDE. The LSV scan is similar to the CV with the only difference being that the LSV only scans in one direction whereas the CV will scan forward in one direction and then reverse directions to scan back to the starting point. An LSV will scan from an initial potential point to a final potential, plotting the current recorded at each point along its path designated by the scan rate. With the decision made to use LSV scans for this system all previously taken CV scans were retaken as LSV scans to allow for

a clear comparison to future scans. So LSV scans were taken at 0rpm, 1000rpm, 1500rpm, 2000rpm, 2300rpm, 2500rpm, and 2800rpm, each at varying scan rates. Each test was taken between the potentials of 0.3V and -0.5V to capture the reduction of Ni2+ at -0.042V. From each test the limiting potential was taken to be used to calculate the concentration of nickel using the Levich equation. The concentration from this calculation would then be compared to the value found with the ICP test. These scans would be compared to the scans taken with blank salt and used to compare to the quaternary salts in the following tests.

After the $LiCl - KCl - 1wt\%NiCl_2$ tests were completed, tests could begin with the quaternary salt, $LiCl - KCl - 1wt\%NiCl_2 - 1wt\%CrCl_2$. To make the salt 0.5020g, or one weight percent, of $CrCl_2$ was added to the $LiCl - KC - 1wt\%NiCl_2$ salt while it was already at operating temperature. The salt was then allowed to sit at temperature overnight in order for it to equilibrate. The next day a sample was taken from the salt to be used in ICP-MS analysis to determine the concentration of both the nickel and chromium in the salt. After a sample was taken the electrodes were inserted into the molten salt and an OCP was run while the system stabilized. Once the OCP showed a stable system LSV scans were run with the RDE stationary. These scans were run between the potentials of 0.3V and -1.0V to ensure that both the nickel and chromium reduction peaks could be seen at -0.042V and -0.732V respectively. Several scans were taken with different scan rates: 20mV/s, 50mV/s, 75mV/s, and 100mV/s. Once the stationary LSVs were completed the RDE was set to rotate at 1000rpm. With the RDE rotating the system was once again allowed to come to equilibrium before more LSV scans were run. The LSVs run using all the same settings that had been used in the static system. From each LSV the limiting potential of both chromium and nickel was determined and used in the Levich equation to calculate the concentration of the two analytes. These concentrations were then compared to the values from the ICP. For both the static and rotating system an OCP scan was run until it showed a stable system

before each LSV was run. After each LSV the RDE was electrochemically cleaned to ensure a fresh working surface.

3.2.2 $LiCl - KCl - EuCl_3 - SmCl_3$

The second experiment done using the graphite RDE was done using LiCl, KCl, $EuCl_3$ (Ultra Dry, 99.99% Alfa Aesar), and $SmCl_3$ (99.9%, Sigma-Aldrich). Here europium and samarium were chosen because their reduction and oxidation potentials are far enough apart from one another so there is no overlap providing a clear curve from which to obtain their limiting potentials. These two salts also have the benefit of having soluble-soluble redox reaction, so running full CV scans, as opposed to the LSVs run in the previous test, is possible. The CV scan will provide a much nicer picture of what is happening in the salt and thus a clearer comparison between static scans and flowing scans. To begin, 22.5720g of LiCl and 27.5084g of KCl were placed in alumina crucible and heated to 300C for eight hours to remove any moisture or other impurities from the salt. The salt was then heated to the desired operating temperature of 450C and left to stabilize overnight. Once the salt had melted a small sample was taken to be used in ICP-MS analysis to check for any significant impurities. Next the RDE, graphite rod, and Ag/AgCl electrodes were immersed in the salt and an OCP scan was started. A new graphite RDE of the same design was used for this set of tests. When the OCP scan showed that the system had come to equilibrium a CV scan was run with the RDE stationary. Several scans with different scan rates were run in the blank salt to check for any impurities in the salt and to ensure that the RDE was working as expected.

After these static scans of the blank salt were complete 0.5190g, or one weight percent, of the $EuCl_3$ was added while the bulk salt was already at operating temperature. The

new $LiCl - KCl - 1wt\%EuCl_3$ was then allowed to come to equilibrium overnight. The next day a sample was taken from the salt to be used in ICP analysis to determine the exact concentration of europium in the salt. The working, counter, and reference electrodes were then inserted into the salt and an OCP was run as the system stabilized without the RDE rotating. When the OCP scan showed a stable system, the electrochemical tests were started. Several CV scans were taken while the RDE was static. The CV was scanned between potentials of 0.8V and -0.1V so that the reduction peak of europium at 0.32V was visible, with scan rates of 10mV/s, 20mV/s, and 35mV/s. After the static scans were complete this procedure was repeated with the RDE rotating at 1000rpm, 1500rpm, 2000rpm, 2200rpm, and 2400rpm with the same scan rates as the static tests. Before each CV scan was completed an OCP scan was run to make sure that the system was at equilibrium and the RDE was electrochemically cleaned to ensure a fresh working surface. The limiting current was then determined from the CV scans and the Levich equation was used to calculate the concentration of europium in the salt. This was then compared to the value provided by the ICP-MS analysis.

Once all the tests were completed with the ternary salt, one weight percent, 0.5266g, of the $SmCl_3$ was added while the salt was already at operating temperature to make $LiCl - KCl - 1wt\%EuCl_3 - 1wt\%SmCl_3$. After allowing the new salt to equilibrate a small sample was taken to be used in ICP-MS analysis to measure the concentration of both europium and samarium in the salt. The RDE, graphite rod, and Ag/AgCl were then placed into the salt and an OCP scan was run while the system came once again to equilibrium. With the system at equilibrium a CV scan was done between the potential of 0.8V and -1.4V so that the reduction potentials of both europium and samarium would be visible. After the first CV scan it was clear that something was not working as expected. Several attempts were made to rectify the issue. The insulation on the rotator shaft was checked and redone and

the back of the furnace was insulated to ensure no contact with the metal rotator stand, as these connections were initially thought to be the cause of the problem. When this did not fix the issue new RDEs were made and tested thinking that the seal might no longer be sufficiently tight. After each alteration to the system a new CV was run to test if the fix had alleviated the problem. None seemed to have any effect on the CV scan.

Chapter 4

Results

4.1 Tungsten RDE

All of the tungsten RDE designs were tested on the rotator before they were tested in the salt system to make sure that they could achieve the smooth rotation that is necessary for laminar flow. The initial design was observed to have a wobbly rotation and did not pass this test. Each of the following designs did display a smooth rotation at high speeds and were subsequently tested in the molten salt system. The first RDE that was tested electrochemically was the one fabricated using a stainless-steel spring as the connection between the graphite and tungsten and sealed using the alumina adhesive. The results from the CV scan taken using this RDE can be seen in Figure 4-1 where it is compared to a CV scan taken using a standard tungsten rod as the working electrode.

The top curve shows a CV scan taken with a traditional tungsten rod as the working electrode. Under static conditions the tungsten RDE should provide the exact same scan. The scan should have zero current except for at the potentials corresponding to the lanthanum and potassium reduction and oxidation peak currents. This is exactly what the top plot shows. The curve that corresponds to the CV taken when using the RDE as the working electrode, the lower curve, shows something very different than expected. Unlike the first curve, the second shows a significant current throughout all of the scanned potentials causing a large slope in the shape of the curve. This current is obscuring the reduction and oxidation

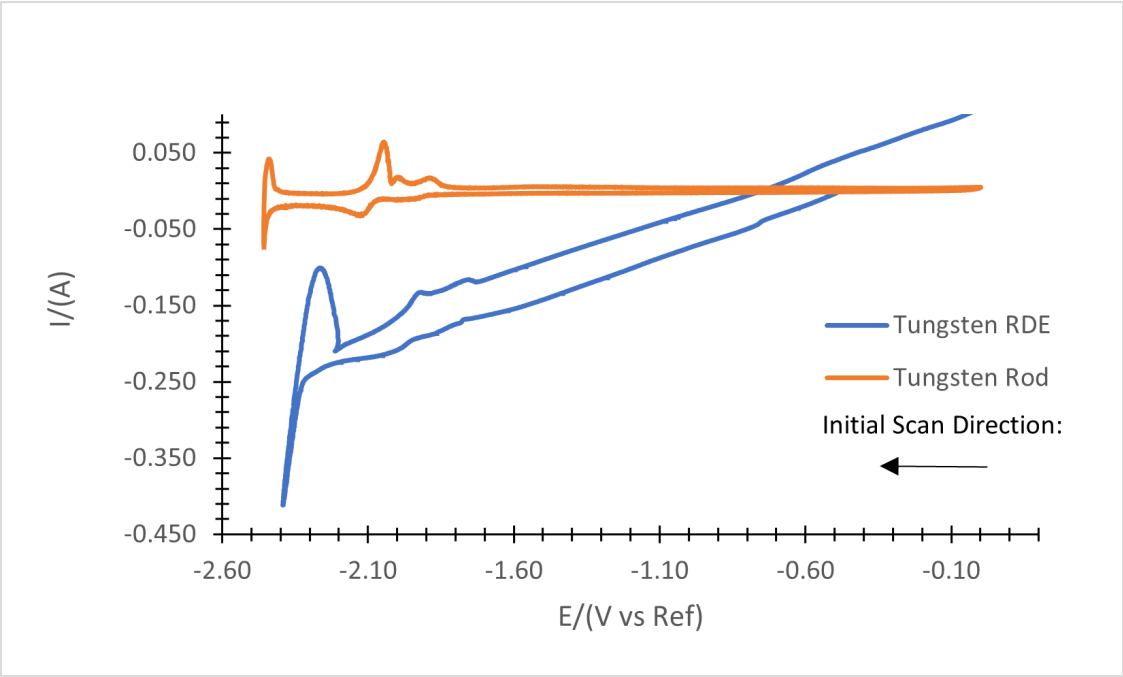

Figure 4.1: CV taken using Tungsten RDE as WE compared to CV taken using Tungsten Rod as WE. 450°C

peaks of lanthanum almost to the point of neither of them being visible, making it impossible to determine the correct current values. Even if the peaks were clear, the additional current would need to be accounted for in any calculations those values would be used in. Considering that the source of the current is unknown it is not possible to take it into account, meaning that any data taken using this RDE design could not be reliable. Since the current is not due to the salt system itself, it must be due to the design and fabrication process of the RDE. In order to determine exactly what was causing the problem, the RDE was taken apart. Here it was seen that the stainless-steel spring that had been holding the tungsten and graphite together had corroded, shown in Figure 4.2. It was then concluded that this spring was what was causing the additional current in the system. Clearly the design needed to be altered to eliminate this problem.

The alterations to the tungsten RDE design consisted of using copper spring instead of

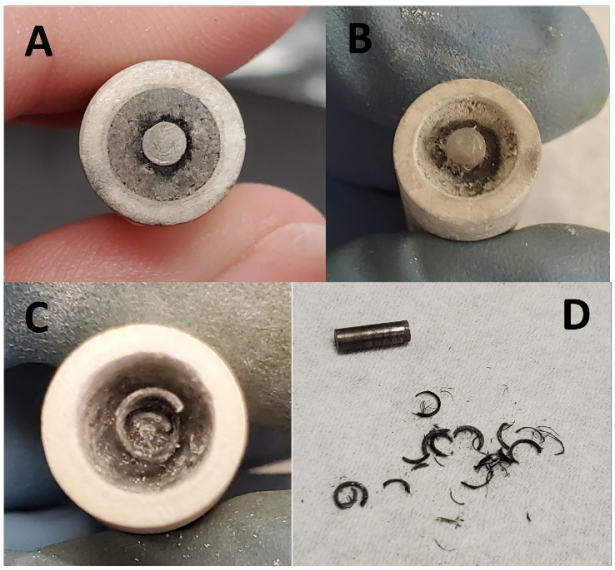

Figure 4.2: RDE with Stainless-steel spring. A: RDE after tests in salt system. B&C: Alumina adhesive has been removed to expose tungsten and stainless-steel spring. D: Corroded stainless-steel spring removed from alumina tube

the stainless-steel spring and a magnesium oxide adhesive instead of the alumina adhesive. The results of the CV scan taken the RDE fabricated in this manner are shown in Figure 4-3, where they are compared to the CV taken with the previous iteration of the design. Curve A shows a CV scan taken with the previous iteration of the tungsten RDE, though taken several days after the scan taken shown in Figure 4-1. In this later scan the reduction and oxidation peaks of lanthanum are no longer visible, suggesting that the degradation of the stainless-steel spring had progressed farther in the days after the initial scan. Curve B scan shows a CV curve taken using the RDE that had been fabricated using a copper wire and magnesium oxide adhesive. Like the first curve the second curve displays a significant current throughout the potential range scanned. It too does not show either the reduction or oxidation peaks for lanthanum. Because both curves show similar currents it is clear that the stainless-steel spring was not the only component of the design that was causing problems. After further study on how the alumina and magnesium oxide adhesive worked, it was determined that when the adhesives had dried they were porous enough to allow

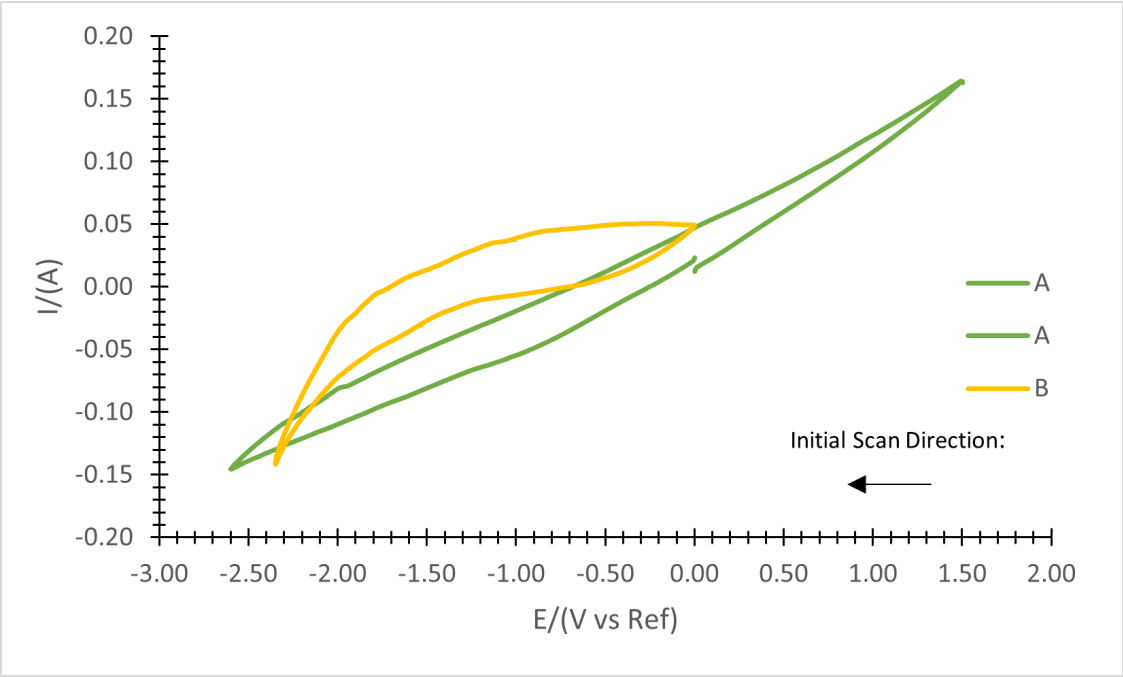

Figure 4.3: CV taken with RDE made with alumina adhesive and stainless-steel spring (A) vs. CV taken with MgO adhesive and copper spring (B). 450°C

the molten salt to seep in and react with the copper wire and the graphite along with the tungsten.

The porosity of the adhesive was dealt with by coating the fully cured RDE in a boron nitride aerosol that should prevent any salt from getting through the adhesive. This method of sealing the RDE was tested on both the magnesium oxide adhesive and the alumina adhesive. A comparison between CV scans taken using coated RDE and an RDE without the coating is shown in Figure 4-4. The first curve shows the CV taken using the RDE fabricated using the MgO adhesive that had not been coated in the BN spray. As before, it displays a large current in the system that is due to the salt seeping in through the unseal adhesive. The second curve shows the CV taken using an RDE that had been fabricated using the MgO adhesive and the BN spray. There is still a fairly significant current throughout the second curve, but it is much less drastic than that seen in the first. While they are

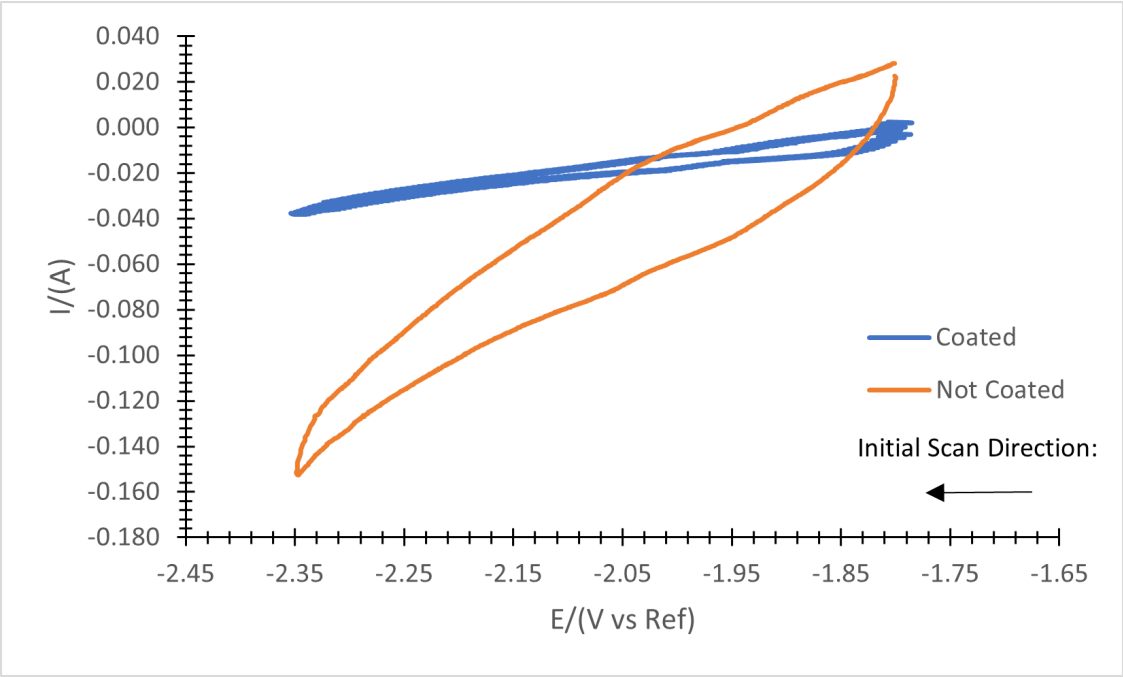

Figure 4.4: CV of BN Coated RDE vs CV of non-BN Coated RDE. 450°C

very slight the oxidation and reduction peaks of lanthanum are visible in the Coated curve where they are not in the Not Coated. The boron nitride seal clearly improved the quality of the CV scans taken with the tungsten RDE, however, the fact that a current still remains prevents the data from being usable. This scan shows that while the RDE design is much improved from its initial concept it still requires a more thorough method of insulation to prevent any salt that does seep through the adhesive from interacting with the copper and graphite.

In order to further ensure that any salt that does manage to seep through the adhesive can't interact with the graphite and copper both were coated in the BN spray before being cemented into the boron nitride tube. This would provide a second layer of protection from the salt and thus should allow the RDE to work as expected. The results of this method of fabrication are shown in Figure 4-5. The lower curve shows the CV taken using the RDE that was fabricated by only coating the adhesive in the boron nitride sealant. The upper curve

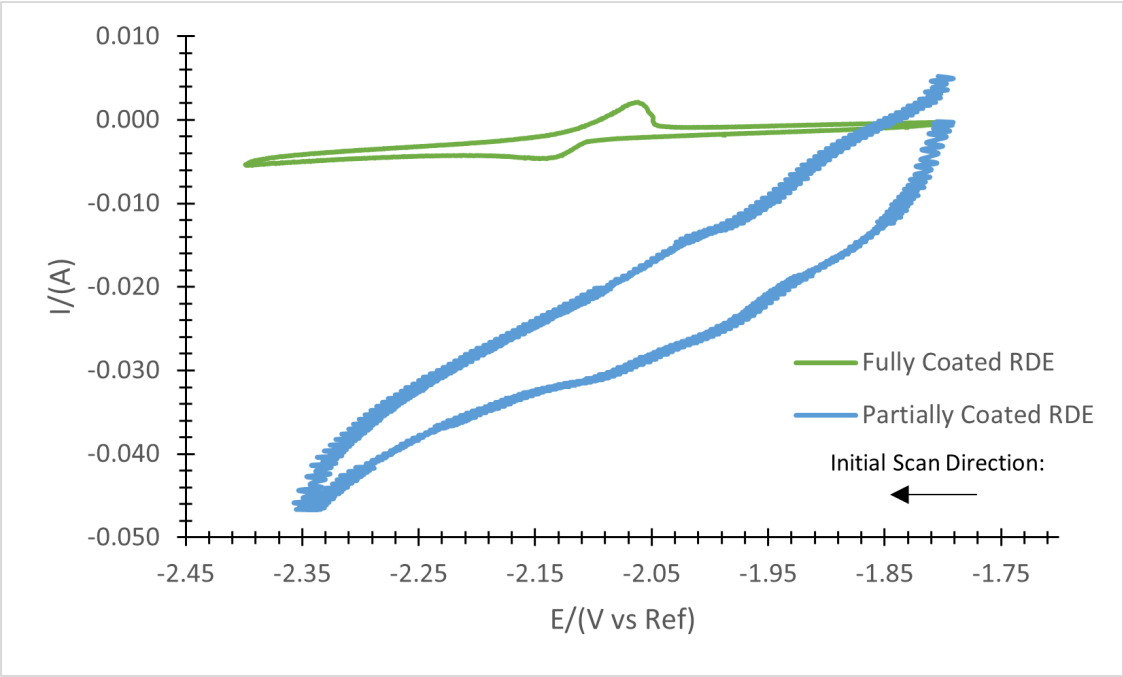

Figure 4.5: CV of Fully Coated RDE vs CV of Partially Coated RDE. 450°C

shows the CV taken using the RDE that had both the inner connections and the adhesive coated with the boron nitride spray. The lower curve still has the large additional current present throughout the scanned potentials, but it is much smaller than without the sealant and the reduction and oxidation peaks are visible. They are still much too obscured by the current caused by the salt seeping through adhesive to be usable, but they are present. There is almost no slope to the top curve, it only drops below the zero point by a few mV making it nearly negligible. This curve is much closer to resembling the CV scan taken with a traditional tungsten rod as the working electrode. Here the reduction and oxidation peaks of lanthanum are very clear and look as though they would provide reliable data for calculating the concentration of lanthanum in the salt. Based on this comparison, it appears that the combination of coating the adhesive and the graphite/tungsten connection within the cement would allow for an RDE that produces reliable data. To test this, several more scans were taken using the RDE that had been fabricated in this manner.

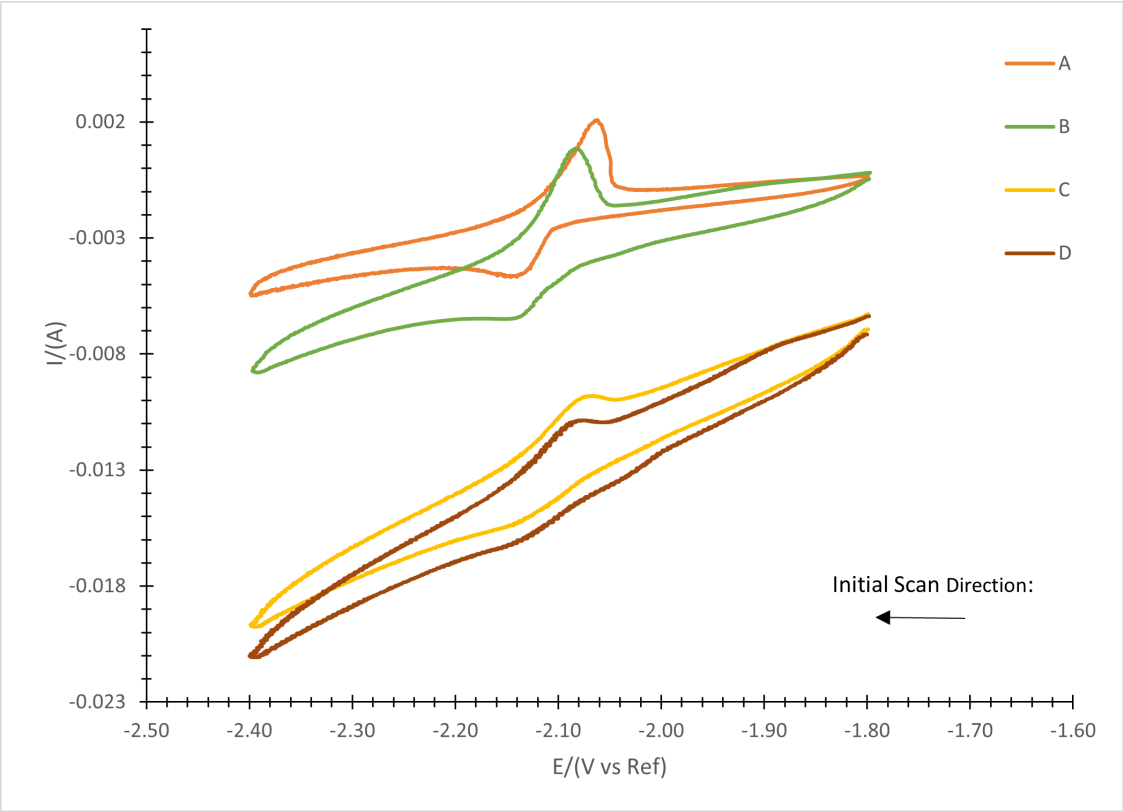

Figure 4.6: CV curves taken with fully coated tungsten RDE. A and B on first day, C and D on second day. 450°C

Several CV scans using the same fully coated RDE were run on the same day. A few days later several more scans were run using that same RDE. After each scan the RDE was electrochemically cleaned. The results of these tests are shown in Figure 4-6. Curve A shows the first CV taken using the fully coated tungsten RDE. The slope caused by the additional current is nearly negligible and the reduction and oxidation peaks are clearly present. A few hours later a second CV was taken using the same RDE and is shown in curve B. The slope is slightly more pronounced than in the previous test and the peaks are slightly less defined, indicating that this set of data may no longer be reliable. Several days later two CV scans were completed using the same RDE used to get curves A and B. These CVs are represented by the two lower curves in Figure 4-6, C and D. Not only is the current much

more pronounced than in the previous curve, but the entire scan has also been shifted down to more negative currents. While the reduction and oxidation peaks are still visible, if only just, they are certainly no longer reliable unless the additional current can be accounted for, which it cannot be. Based on these four curves it is clear that while coating both the inside and the outside of the tungsten RDE in the BN spray does provide for a deceptively reliable CV curve, it only lasts for a short time before that salt is able to make its way past both the boron nitride spray and the adhesive.

4.2 Graphite RDE

4.2.1 $LiCl - KCl - NiCl_2 - CrCl_2$

After it was determined that the tungsten RDE was not able to produce reliable results all further tests were completed using the graphite RDE. The first set of tests were done in $LiCl - KCl - NiCl_2$, both in the static case and in the flowing case. Figure 4.7 shows the results of using the graphite RDE as the working electrode in the static case, with an Ag/AgCl reference electrode and a graphite counter. As expected, the curves show zero current at all potentials except for those that correspond to the reduction and oxidation potentials of the nickel in the salt. Here since the only reaction is the Ni^{2+} reducing to Ni there is only a single peak visible in each scan. This curve indicates that the graphite RDE is working exactly as expected, giving results no different from what a traditional graphite rod would produce. It is also worth noting, in further evidence that the RDE is working correctly, that the peak current is dependent on the scan rate used during the CV, as suggested by the Berzins-Delahay equation. As the scan rate increases, the height of the oxidation and reduction peaks also increases. With proof that the graphite RDE does in fact provide good

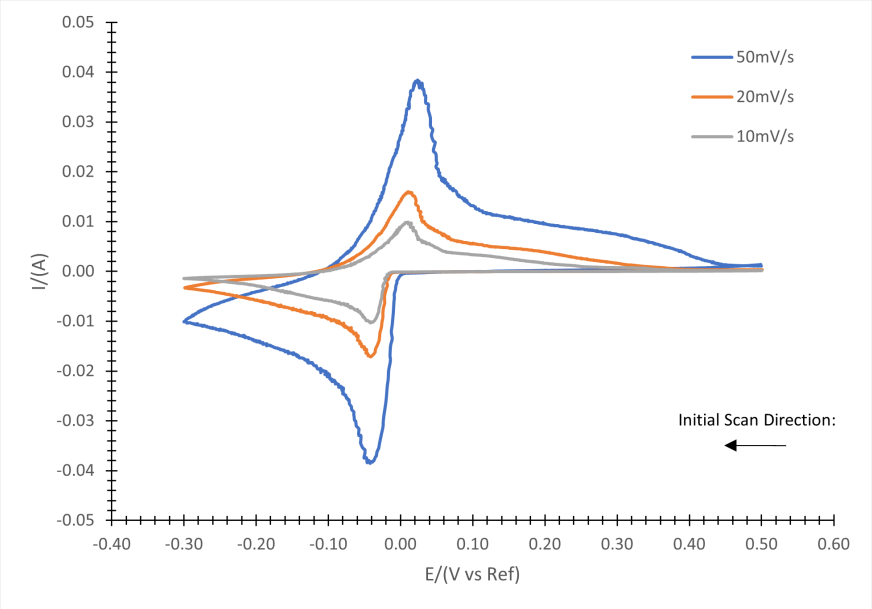

Figure 4.7: CV of LiCl-KCl-NiCl2 using Graphite RDE as WE, Ag/AgCl reference, graphite Counter, 0rpm, 450°C

data, the RDE was rotated at different rates to examine what effects this might have on the CV scans and concentration measurements.

Unfortunately, when the RDE was rotating at the desired speeds it became apparent that running a full CV scan would not provide for usable data because of nickel's soluble-insoluble redox reaction. Instead LSV scans were used to collect the desired data when the RDE was in motion. The LSV scans taken using the RDE in the $LiCl - KCl - NiCl_2$ system are shown in Figure 4.8. This figure shows four different LSV curves, each taken at a different rotating rate with the same scan rate every time. The rotation rate was increased from 1500rpm to 2800rpm. Each of the four scans were taken in the same salt as that used in the static case with the same RDE. The surface of the RDE was electrochemically cleaned between each test. Unlike the stationary scans, LSV scans taken in a flowing system do not display current peaks at the reduction potential, instead they show a limiting current plateau. Both the peak current from a static scan and the limiting current plateau from a

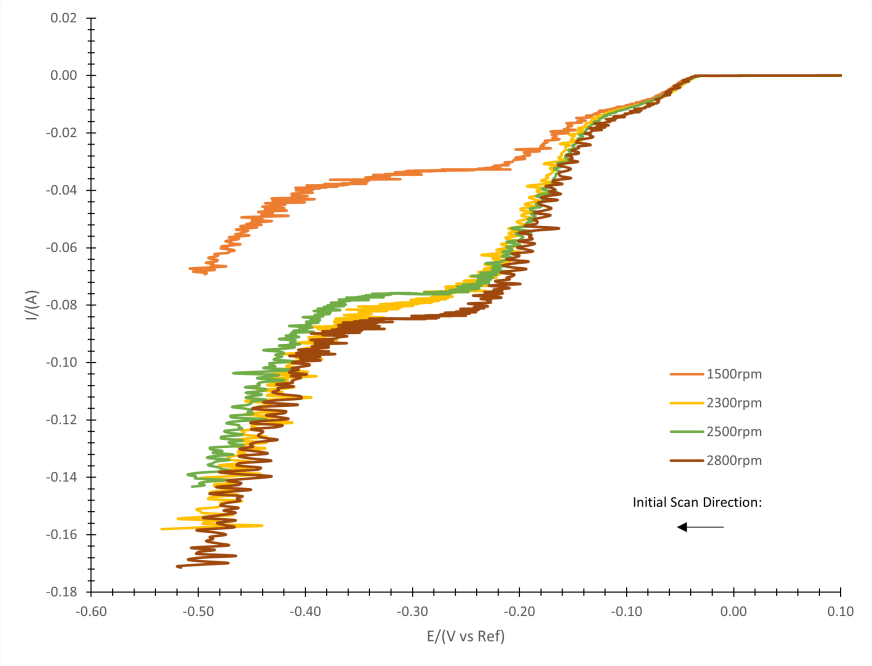

Figure 4.8: LSV with graphite RDE in LiCl-KCl-NiCl2, scan rate 20mV/s, reference: Ag/AgCl, counter: graphite, 450°C

flowing scan should be at the same potential for the same system. Additionally, there should only be one limiting current in a flowing system for every peak current seen in a static scan. This is not what is shown in Figure 4.8. These curves each show two plateaus where only one was expected based on the salt composition and the results of the static case. One of the plateaus is at nickel's reduction potential and matches what is expected from when the RDE was not rotating. The second plateau, however, was completely unexpected. The static scan gave no indication that there is a second reaction happening in the system at that potential. When the salt was analyzed using ICP-MS there were no impurities in the salt that would account for this. Given this information, it seems only possible that the additional plateau is due to the formation of $(NiCl_4)^{2-}$ and its subsequent reduction [42].

Since we know that the first plateau corresponds to the reduction of Ni^{2+} to Ni, that is the curve that was focused on for concentration measurement. While this plateau is not

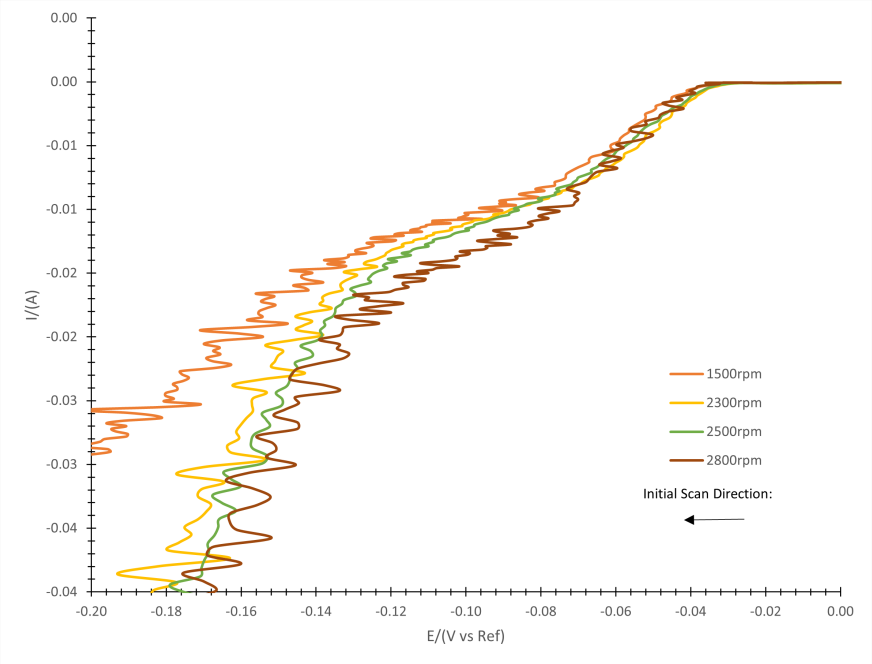

Figure 4.9: LSV scan using Graphite RDE in LiCl-KCl-NiCl2. Zoomed in on the Ni2+ reduction plateau. 450°C

perfectly flat it is still possible to estimate the limiting current with a high degree of certainty. This current value was then used in the Levich equation to calculate the concentration of nickel in the salt. The limiting potential from the 1500rpm curve is 10.87mA. Using this information, along with nickel's diffusion coefficient in LiCl-KCl of $1.1 \times 10^{-5} cm^2/s$ [31] and the systems kinematic viscosity of $0.0413 cm^2/s$ [18], the concentration of nickel in the system was calculated to be 0.370wt%. The concentration of nickel in the salt was also determined via ICP-MS analysis and with this method was found to be 0.369wt%. These two values are extremely close, indicating both that the RDE is working in the desired/expected manner and that the first plateau is indeed the one that corresponds to the reduction of nickel

After confirming that the graphite RDE works as expected in the tertiary salt, one weight percent of $CrCl_2$ was added to the existing salt system to make $LiCl-KCl-NiCl_2-CrCl_2$. The RDE was tested in this salt system first with zero rotation and then at 1000rpm. The

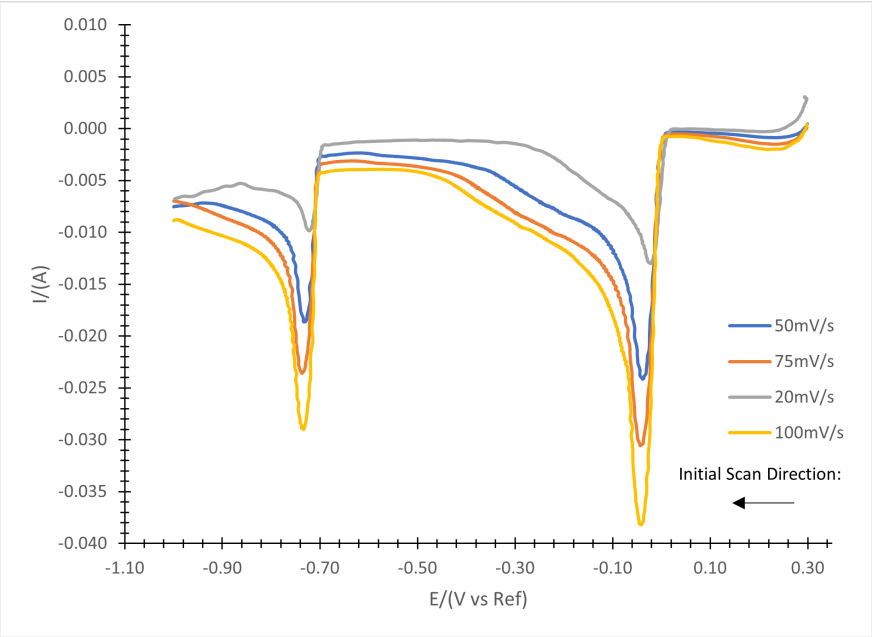

Figure 4.10: LSV using Graphite RDE in LiCl-KCl-NiCl2-CrCl2, reference:Ag/AgCl, counter:graphite, 0rpm, 450°C

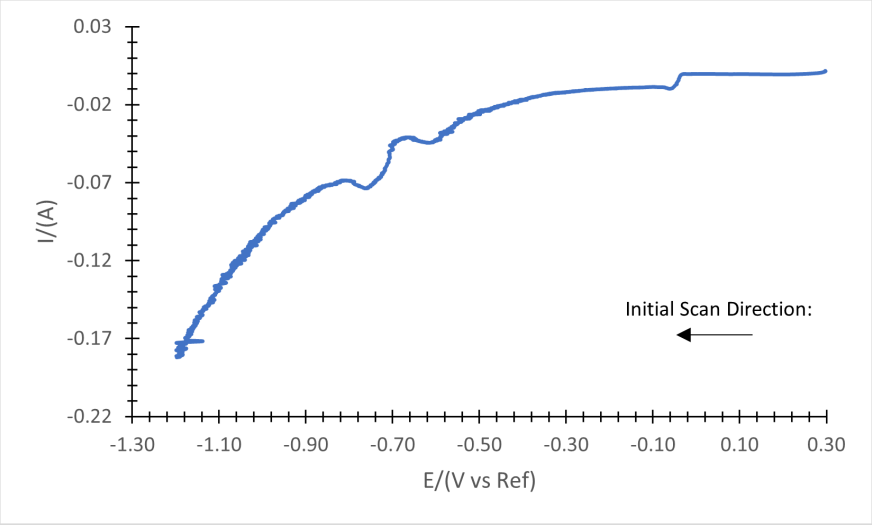

Figure 4.11: LSV using Graphite RDE in LiCl-KCl-NiCl2-CrCl2, reference:Ag/AgCl, counter:graphite, scan rate: 75mV/s, 1000rpm, 450°C

LSV scans taken in the static system came out exactly as expected and are shown in Figure 4.10. There are two peaks, one corresponding to the reduction of nickel and the second representing the reduction of chromium. As with the tertiary salt, the peak current height for both analytes increases with increasing scan rate in accordance with the Berzins-Delahay equation. Figure 4.11 then shows the results of LSV scans taken while the RDE was rotating at 1000rpm. Once again, this scan shows one more plateau than was expected based off of the peaks in the stationary case. The first plateau represents the reduction of nickel in the salt and corresponds to the first peak in the static scans. The second reaction is believed to be the reduction of $(NiCl_4)^{2-}$ that was seen in the tertiary salt. Finally, the third plateau corresponds to the chromium reduction in the system. Note that since the RDE is flowing during this scan the reactions should be represented by plateaus rather than the peaks seen in the static case. In Figure 4.11 the reactions seem to show a combination between the limiting current plateau and the peak current peaks. This is likely because of the high scan rate used in this test. Were the scan rate to decrease the curve would slowly lose the peak shape in favor of a pure plateau [34]. From this curve the limiting currents of both the nickel and chromium were taken and used in the Levich equation to calculate the concentration of each in the salt. The nickel concentration was found to be 0.409wt%, using the limiting current of 9.81mA and the diffusion coefficient of $1.1 \times 10^{-5} cm^2/s$ [31]. This value compared well to the concentration found by ICP-MS analysis, which was 0.369wt%. The chromium concentration was calculated to be 0.635wt%, using the limiting current of 18.355mA and the diffusion coefficient of $1.21 \times 10^{-5} cm^2/s$ [30]. Unlike the nickel concentration, this value varied widely from that found during the ICP-MS analysis, 0.407wt%. Both the nickel and the chromium concentrations were calculated using a system kinematic viscosity of $0.0412 cm^2/s$ [18] and a rotation rate of 1000rpm. The discrepancy in the chromium concentrations can be explained by the large curve seen in the LSV scan. After the nickel reduction the current begins to gradually drop off as it moves toward the second and third reactions. This decrease in current

would be due to the increase in the working electrode's, RDE's, surface area, which is due to the deposition of nickel on the graphite disk of the RDE. With the nickel deposited on the graphite surface it becomes impossible to obtain reliable data by the time the chromium potential comes around.

4.2.2 $LiCl - KCl - EuCl_3 - SmCl_3$

Once it was clear that the nickel-chromium system would not provide the results we were looking for in this study a different salt system was chosen. The next set of tests would be run in $LiCl - KCl - EuCl_3 - SmCl_3$. To begin with the RDE was tested first with zero rotation in just $LiCl - KCl - EuCl_3$. An entirely new RDE, of the same design, was used for these tests. The results of these tests are shown in Figure 4.12. Unlike in the nickel/chromium system of the previous tests, it is possible to take full CV scans in this system because the europium has a soluble-soluble redox reaction, allowing for a clear, smooth curve at the desired potentials. This will provide for a much clearer picture of how the system works and how the flowing and static cases differ. The figure shows three CV curves each taken at different scan rates. In accordance with the Randles-Sevcik equation, the height of the peak currents increases with an increase in the scan rate. As expected, based on the composition of the salt there is only a single reduction and oxidation peak visible in these curves. This peak corresponds to the reduction of Eu^{3+} to Eu^{2+}. Had the scan been taken to more negative potentials the reduction of Eu^{2+} to Eu would have also been visible. We are only interested in the one reaction for this study however, so only the potential range for the first reaction is examined. With the static scan as evidence that the graphite RDE used for these tests was working correctly, the flowing tests were started.

The RDE was rotated at rates between 1500rpm and 2400rpm, with scans taken at each

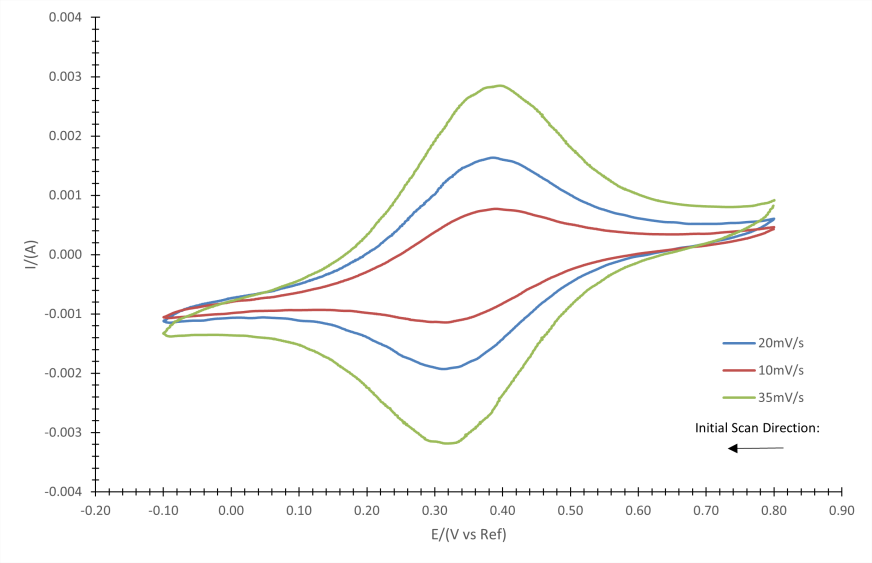

Figure 4.12: CV in $LiCl-KCl-1wt\%EuCl_3$, working: graphite RDE, reference: Ag/AgCl, counter: graphite, 0rpm, 450°C

speed using three different scan rates. Those scan rates were 10mV/s, 20mV/s, and 35mV/s. The results of these scans are shown in Figure 4.13 and Figure 4.14. Figure 4.13 shows three CV scans all taken at the same rotation rate but done using different scan rates. As expected, the limiting current is located at the same potential as the peak current in the static scan and there is only a single plateau as opposed to the multiple seen in the previous tests. Unlike the static case, however, the height of the limiting current plateau is not dependent on the scan rate of the CV tests. For each of the three scans done at this rotation rate, the limiting current plateau falls at roughly the same height.

Figure 4.14 shows five different CV scans taken with the graphite RDE at rotation rates ranging from 1500rpm to 2400rpm, all done using the same scan rate of 10mV/s. As is suggested by the Levich equation the height of the limiting current is dependent on the rotation rate of the electrode. When the rotation rate is increased the limiting current becomes increasingly more negative. From these scans it is possible to obtain a clear limiting current value for each rotation rate. Using the Levich equation, the limiting current value,

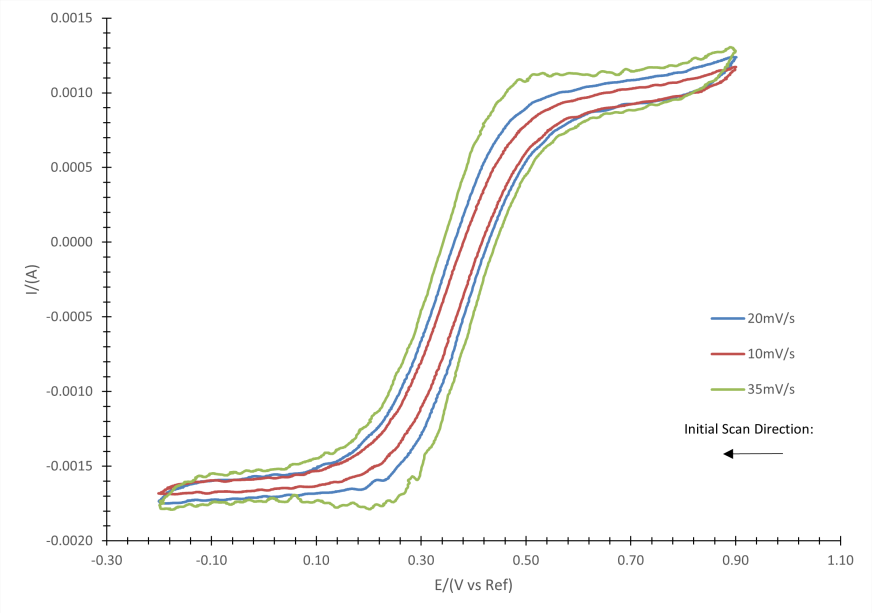

Figure 4.13: CV in $LiCl - KCl - 1wt\%EuCl_3$, working: graphite RDE, reference:Ag/AgCl, counter:graphite, 2000rpm, 450°C

europium's diffusion coefficient of $9.2 \times 10^{-6} cm^2/s$ [26], and the system's kinematic viscosity of $0.0412 cm^2/s$ [18] it is possible to calculate the concentration of europium in the salt. For example, the reduction limiting current from the 2000rpm curve is 2.527mA. This gives a Eu^{3+} concentration of 0.434wt%. From the oxidation plateau and Eu2+'s diffusion coefficient of $5.1 \times 10^{-6} cm^2/s$ [7] we can calculate the concentration of Eu2+. The oxidation limiting current from the 2000rpm curve is 1.047mA, which gives a Eu2+ concentration of 0.133wt%. Combining these two gives a total europium concentration of around 0.567wt%. From the ICP analysis of this salt, the concentration of europium was found to be 0.514wt%, which matches well with the calculated results. Similar results could be calculated for each of the five different rotation speeds and compared to the ICP results.

With the tests from the ternary salt completed and analyzed, one weight percent of $SmCl_3$ was added to the salt system. After allowing the system to come to equilibrium CV scans were run using the same graphite RDE that had been used in the ternary salt. The RDE

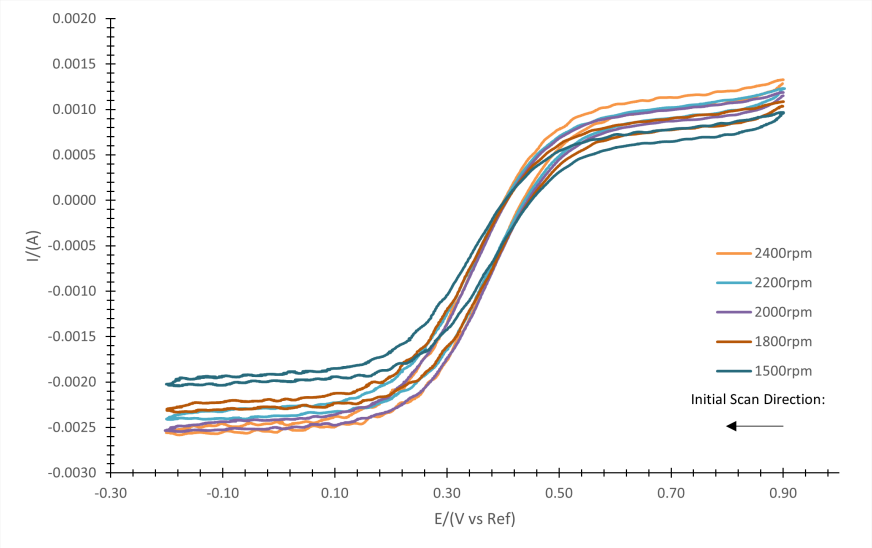

Figure 4.14: CV in $LiCl - KCl - 1wt\%EuCl_3$, working: graphite RDE, reference:Ag/AgCl, counter:graphite, scan rate: 10mV/s, 450°C

had been electrochemically cleaned before being used in the new tests. The first scans done were done with the RDE stationary so that there was no flow in the system. It was expected that the CV curves would come out similar to the CVs taken with the ternary salt, only with an additional peak. That there would be two clearly defined peaks, one at the europium potential and another at the samarium potential. The curves, however, did not come out exactly as expected. The results of the first set of tests in this salt are shown in Figure 4.15.

The europium peak is visible at the correct potential, but it is not nearly as defined as it was in the ternary salt and there is a sharp upward slope coming off of the tail of the oxidation peak where it should be dropping back down to zero. The samarium peak should be located around -0.8V. At this potential there are two very poorly defined peaks in the curve, but they are not nearly clear enough to provide any usable data. In between the two reactions the curve should come to zero on both the forward and back scan. While the back scan does come to zero the forward scan is well below this point. Even though the back scan looks to have a zero current between the two reactions it is not a smooth curve. There are

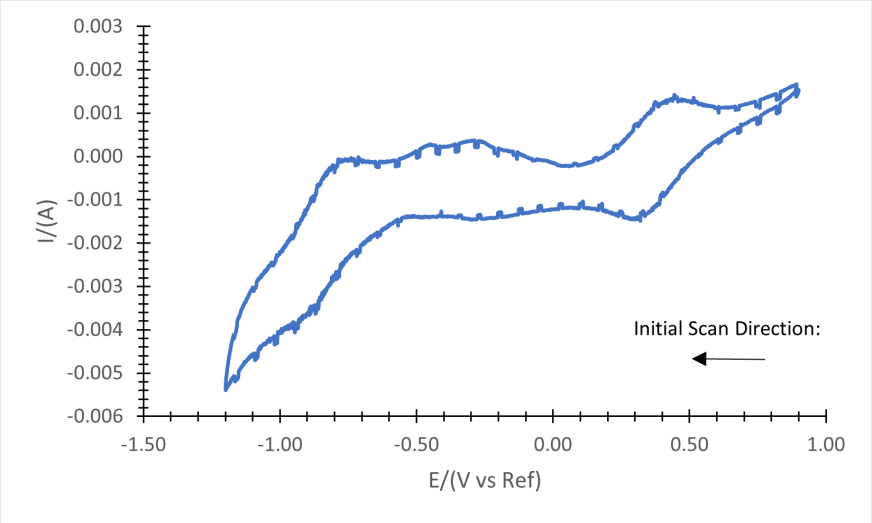

Figure 4.15: CV in $LiCl - KCl - 1wt\%EuCl_3 - 1wt\%SmCl_3$, working: graphite RDE, reference:Ag/AgCl, counter:graphite, scan rate: 20mV/s, 0rpm, 450°C

several, small additional peaks in that range and the current drops below zero before rising to the europium peak. Perhaps the strangest part of this curve is that the oxidation peak of samarium is at a negative current. Combined, all of these unexpected features of the curve strongly indicate that there was something wrong with the system. At first it was thought either the salt had been contaminated or the RDE had broken. After several attempts to fix these problems, it became clear that the actual problem was most likely resulting from a connectivity issue. Perhaps the rotator shaft had not been properly insulated or there was some unwanted contact with the electrodes or their connections. Ultimately, we were unable to determine what exactly was causing the problem with the curves.

Chapter 5

Discussion/Conclusions

5.1 Tungsten RDE

In this work, a design for a tungsten rotating disk electrode was created. The design was meant to be relatively cheap and simple to fabricate. Many of the current designs for rotating electrodes are either not suitable to high temperature, corrosive environments, or are difficult and costly to fabricate. The tungsten RDE design was meant to be used in high temperature molten salt systems to be used in electrochemical studies of the salt. Unlike the few rotating electrode designs that have been presented in other works, this one was created to be easier to fabricate as it would require far less precision measurements. This is one of the main reasons a rotating disk electrode was chosen over a rotating ring or cylinder electrode. In general, they are much easier to make. Several attempts and alterations were made in hopes of creating a successful RDE before it was decided that no iteration of this design would produce the desired results. The first iteration of the tungsten RDE was dismissed before it was ever tested in the salt system due to its wobbly rotation. Each subsequent design showed a smooth rotation and was then tested in the electrochemical cell. The first three alterations to the initial design did not produce CV scan even close to what was expected based on the CV scans taken with a traditional tungsten rod under the same conditions. Each RDE was tested in $LiCl - KCl - LaCl_3$, meaning that in the potential range scanned the reduction and oxidation peaks of lanthanum should have been visible. This was not

the case. On top of the peaks not appearing there was an additional unexpected current throughout the potential range when the current should have zero. It was believed that this current was the reason that the reduction/oxidation peaks were not visible in the scan and that it was caused by the salt seeping through the adhesive. The final alteration to this tungsten RDE was to coat the connection between the graphite and tungsten in a boron nitride coating along with the outer layer of adhesive once it had fully cured. This change finally insulated the electrode material enough to allow the oxidation and reduction reactions of the lanthanum to be visible in the CV scans. However, the current was still apparent, if much decreased, and the longer the RDE was in the salt the larger the current became and the less clear the reduction/oxidation peaks appeared. It seemed that the boron nitride coating could only protect the electrode for a short while and was ultimately not the solution to the tungsten RDE problem. With no further solutions in sight, it was decided to move on from the tungsten RDE and focus further studies on the design and use of a graphite RDE.

5.2 Graphite RDE

Two sets of experiments were done using a graphite RDE designed in this work. The graphite RDE was fabricated using a piece of graphite that had been cut into the desired size and shape and then fit snugly into a boron nitride tube. When heated the graphite's larger thermal expansion coefficient would cause a tight seal between the boron nitride tube and the graphite to prevent any salt from seeping into the insulation. As an extra preventative a small amount of alumina adhesive was placed between the base of the graphite and tube to ensure that the RDE stayed together even when not at operating temperatures. The exposed base of the graphite was also coated in a boron nitride aerosol to protect it against any accidental contact with the salt.

The graphite RDE was first tested in a $LiCl - KCl - NiCl_2$ salt with zero rotation to make sure that it was working properly. The CV curve obtained with the static RDE showed the same curve one would get using a traditional graphite working electrode, indicating that it did indeed work properly. Once proven to produce reliable results the RDE was rotated at rates between 1500rpm and 2800rpm and LSV scans were run at each rate with several different scan rates. Unlike the static case which showed the expected single peak for the reduction of the nickel, the flowing scans displayed two limiting current plateaus. One clearly corresponded to the reduction of Ni^{2+} to Ni and was the expected reaction. The second plateau was completely unexpected and ultimately determined to be caused by the formation of $(NiCl_4)^{-2}$ and its subsequent reduction [42]. From these LSV scans the limiting current of the nickel reduction was obtained to be 10.87mA at a rotation rate of 1500rpm and used in the Levich equation to calculate the concentration of nickel in the salt. The concentration calculated in the manner was 0.370wt%, which compares well to the value found from ICP-MS analysis of 0.369wt%. With this further evidence the graphite RDE works exactly as expected, it was then tested in the $LiCl - KCl - NiCl_2 - CrCl_2$ salt. Again, it was first tested with zero rotation and presented an LSV curve similar to those expected of the same salt when using a traditional graphite rod electrode. From there the RDE was set to rotate at 1000rpm and several LSV scans were taken at different scan rates. The curve obtained from this test was similar to those from the ternary salt. There were the two expected plateaus that corresponded to the reduction of nickel and chromium, but there was also the additional reaction in between those two due to the $(NiCl_4)^{-2}$ reaction. The nickel and chromium limiting currents collected from this data were 9.81mA and 18.355mA respectively, leading to a nickel concentration of 0.409wt% and a chromium concentration of 0.635wt%. The concentrations of nickel and chromium obtained from ICP-MS analysis were 0.369wt% and 0.407wt% respectively. The discrepancy between the calculated concentration of chromium and the measured value was determined to be due to nickel deposition on the

working electrode surface, thus increasing the working surface area making it impossible to accurately calculate the chromium concentration.

The second set of tests done using the graphite RDE were done in $LiCl - KCl - EuCl_3$ and $LiCl - KCl - EuCl_3 - SmCl_3$. Initially the graphite RDE was tested in the $LiCl - KCl - EuCl_3$ salt under static conditions with three different scan rates. Once again, the CV curves obtained closely resembled those done with a traditional graphite electrode, clearly showing the europium reduction and oxidation peaks. The RDE was then rotated at rates ranging from 1500rpm to 2400rpm, each at three different scan rates. The concentration of europium was calculated from the 2000rpm curve using the reduction limiting current of 2.527mA for Eu^{3+} and an oxidation limiting current of 1.047mA for Eu^{2+} and the Levich equation.This method obtained an Eu^{3+} of 0.434wt% and an Eu^{2+} concentration of 0.133wt%. These two concentrations combined give a total europium concentration of 0.567wt%, which compares well with the concentration obtained from the ICP-MS analysis of 0.514wt%. One weight percent of $SmCl_3$ was then added to the ternary salt to make the $LiCl - KCl - EuCl_3 - SmCl_3$. Initially the same graphite RDE was used in these tests as was used in the previous, along with the same salt with only the additional $SmCl_3$. When tests were run using this set up with the RDE stationary, the CV curves did not come out exactly as expected. Both the europium and samarium reduction and oxidation peaks were visible but not as clear as expected. The base current was not at zero as it should have been, and the oxidation peak of samarium was below the zero line when it should have been well above. The salt and the RDE were replaced with fresh ones in hopes of eliminating the problem. When this did not result in clearer CV scans the connections at each of the electrodes were checked along with the connection cable to the potentiostat. While none of this produced any answers as to what was causing the poor curves, it was ultimately determined that the problem was being caused by a connection issue that we were not able to discern. At this point work is

continuing to be done in hopes of finding the cause of the problem so that it might be fixed and tests with the graphite RDE can be continued.

Bibliography

[1] Molten salt reactor. https://en.wikipedia.org/wiki/Molten_salt_reactor.

[2] *Methods Involving Forced Convection - Hydrodynamic Methods*, chapter 9, pages 331–364. John Wiley & Sons, Ltd, 2001. ISBN 978-0-471-04372-0.

[3] U.S. Energy Information Administration. Nuclear explained: U.s. nuclear industry. https://www.eia.gov/energyexplained/nuclear/us-nuclear-industry.php.

[4] World Nuclear Association. Outline history of nuclear energy. https://world-nuclear.org/information-library/current-and-future-generation/outline-history-of-nuclear-energy.aspx, .

[5] World Nuclear Association. Molten salt reactors. https://world-nuclear.org/information-library/current-and-future-generation/molten-salt-reactors.aspx, .

[6] World Nuclear Association. Nuclear power in the world today. https://world-nuclear.org/information-library/current-and-future-generation/nuclear-power-in-the-world-today.aspx, .

[7] M.R. Bermejo, F. de la Rosa, E. Barrado, and Y. Castrillejo. Cathodic behaviour of europium (iii) on glassy carbon, electrochemical formation of al4eu, and oxoacidity reactions in the eutectic licl–kcl. *Journal of Electroanalytical Chemistry*, 603(1):81–95, 2007. ISSN 1572-6657. doi: https://doi.org/10.1016/j.jelechem.2007.01.018. URL https://www.sciencedirect.com/science/article/pii/S0022072807000514.

[8] Krista Carlson, Levi Gardner, Jeremy Moon, Brian Riley, Jake Amoroso, and Dev Chidambaram. Molten salt reactors and electrochemical reprocessing: synthesis and chemical durability of potential waste forms for metal and salt waste streams. *International Materials Reviews*, 66(5):339–363, 2021. doi: 10.1080/09506608.2020.1801229. URL https://doi.org/10.1080/09506608.2020.1801229.

[9] P. M. Copham and D. J. Fray. The use of rotating electrodes in the electrolysis of molten zinc chloride electrolytes. *Metallurgical Transactions B*, 21:977–985, 1990. doi: https://doi.org/10.1007/BF02670268. URL https://link.springer.com/article/10.1007/BF02670268#citeas.

[10] S. Delpech, E. Merle-Lucotte, D. Heuer, M. Allibert, V. Ghetta, C. Le-Brun, X. Doligez, and G. Picard. Reactor physic and reprocessing scheme for innovative molten salt reactor system. *Journal of Fluorine Chemistry*, 130(1):11–17, 2009. ISSN 0022-1139. doi: https://doi.org/10.1016/j.jfluchem.2008.07.009. URL https://www.sciencedirect.com/science/article/pii/S0022113908002054. Fluorine & Nuclear Energy.

[11] M. Eisenberg, C. W. Tobias, and C. R. Wilke. Ionic mass transfer and concentration polarization at rotating electrodes. *Journal of The Electrochemical Society*, 101(6):306, 1954. doi: 10.1149/1.2781252. URL https://doi.org/10.1149/1.2781252.

[12] Noemie Elgrishi, Kelley J. Roundtree, Brian D. McCarthy, Eric S. Roundtree, T. Eisenhart, Thomas, and Jillian L. Dempsey. A practical beginner's guide to cyclic voltammetry. *Journal of Chemical Education*, 95:197–206, 2018. doi: https://doi.org/10.1021/acs.jchemed.7b00361. URL https://pubs.acs.org/doi/10.1021/acs.jchemed.7b00361.

[13] Zhange Feng, Nicholas S. Georgescu, and Daniel A. Scherson. Rotating ring-disk electrode method for the detection of solution phase superoxide as a reaction inter-

mediate of oxygen reduction in neutral aqueous solutions. *Analytical Chemistry*, 88: 1088–1091, 2016. doi: https://doi.org/10.1021/acs.analchem.5b04346. URL https://pubs.acs.org/doi/10.1021/acs.analchem.5b04346.

[14] Charles W. Forsberg and Ehud Greenspan. Molten salt reactors (msrs): Coupling spent fuel reprocessing and actinide burning. https://technicalreports.ornl.gov/cppr/y2001/pres/118013.pdf.

[15] D. R. Gabe. Review: The rotating cylinder electrode. *Journal of Applied Electrochemistry*, 4:91–108, 1974.

[16] D. R. Gabe and F. C. Walsh. The rotating cylinder electrode: A review of development. *Journal of Applied Electrochemistry*, 13:3–21, 1983. doi: https://doi.org/10.1007/BF00615883. URL https://link.springer.com/article/10.1007/BF00615883.

[17] D. R. Gabe, G. D. Wilcox, J. Gonzalez-Garcia, and F. C. Walsh. The rotating cylinder electrode: Its continued development and application. *Journal of Applied Electrochemistry*, 28:759–780, 1998. doi: https://doi.org/10.1023/A:1003464415930. URL https://link.springer.com/article/10.1023/A:1003464415930.

[18] Jianbang Ge, Jaewoo Park, Amanda Leong, and Jinsuo Zhang. In situ electrochemical study of the coexistence of eu^{3+} and eu^{2+} in molten LiCl-KCl by rotating disc electrode. *Journal of The Electrochemical Society*, 167(16):163506, dec 2020. doi: 10.1149/1945-7111/abd2da. URL https://doi.org/10.1149/1945-7111/abd2da.

[19] J.C. Gomez-Vidal and E. Morton. Castable cements to prevent corrosion of metals in molten salts. *Solar Energy Materials and Solar Cells*, 153:44–51, 2016. ISSN 0927-0248. doi: https://doi.org/10.1016/j.solmat.2016.04.009. URL https://www.sciencedirect.com/science/article/pii/S092702481630023X.

[20] Shaoqiang Guo, Evan Wu, and Jinsuo Zhang. Investigation of electrochemical kinetics for la(iii)/la reaction in molten liclkcl eutectic salt using potentiometric polarization. *Journal of Nuclear Materials*, 510:414–420, 2018. ISSN 0022-3115. doi: https://doi.org/10.1016/j.jnucmat.2018.08.036. URL https://www.sciencedirect.com/science/article/pii/S0022311518307967.

[21] D. Horvath and M. F. Simpson. Electrochemical monitoring of ni corrosion induced by water in eutectic LiCl-KCl. *Journal of The Electrochemical Society*, 165(5):C226–C233, 2018. doi: 10.1149/2.0391805jes. URL https://doi.org/10.1149/2.0391805jes.

[22] V. V. Ignatiev, M. V. Kormilitsyn, L. A. Kormilitsyna, Yu. M. Semchenkov, Yu. S. Fedorov, O. S. Feinberg, O. V. Kryukov, and A. V. Khaperskaya. Molten-salt reactor for nuclear fuel cycle closure on all actinides. *Atomic Energy*, 125(5), 11 2019. doi: 10.1007/s10512-019-00481-w. URL https://link.springer.com/article/10.1007/s10512-019-00481-w.

[23] Tadashi Inoue and Lothar Koch. Development of pyroprocessing and its future direction. *Nuclear Engineering and Technology*, 40:183–190, 04 2008.

[24] Phillips J., R. J. Gale, R. G. Wier, and R. A. Osteryoung. Glassy carbon rotating ring-disc electrode for molten salt studies. *Analytical Chemistry*, 48:1266–1268, 1976. doi: https://doi.org/10.1021/ac50002a053. URL https://pubs.acs.org/doi/abs/10.1021/ac50002a053.

[25] Zheng Jia, Geping Yin, and Jiujun Zhang. 6 - rotating ring-disk electrode method. In Wei Xing, Geping Yin, and Jiujun Zhang, editors, *Rotating Electrode Methods and Oxygen Reduction Electrocatalysts*, pages 199–229. Elsevier, Amsterdam, 2014. ISBN 978-0-444-63278-4. doi: https://doi.org/10.1016/B978-0-444-63278-4.00006-9. URL https://www.sciencedirect.com/science/article/pii/B9780444632784000069.

[26] Tack-Jin Kim, Yong-Ju Jung, S.J. Kim, Seung-Woo Paek, and Do-Hee Ahn. Elucidation of electrode reaction of eucl3 in licl-kcl eutectic melts through cv curve analysis. *Bulletin of the Korean Chemical Society*, 32, 03 2011. doi: 10.5012/bkcs.2011.32.3.863.

[27] J.J. Laidler, J.E. Battles, W.E. Miller, J.P. Ackerman, and E.L. Carls. Development of pyroprocessing technology. *Progress in Nuclear Energy*, 31(1):131–140, 1997. ISSN 0149-1970. doi: https://doi.org/10.1016/0149-1970(96)00007-8. URL https://www.sciencedirect.com/science/article/pii/0149197096000078. The Technology of the Integral Fast Reactor and its Associated Fuel Cycle.

[28] Kui Liu, Yue Ma, Mingliang Kang, and Biao Wang. Facile visualization of the initial nucleation and growth of an active metal electrodeposited in a high temperature molten salt using a detachable disk electrode. *Electrochemistry Communications*, 117:106780, 2020. ISSN 1388-2481. doi: https://doi.org/10.1016/j.elecom.2020.106780. URL https://www.sciencedirect.com/science/article/pii/S1388248120301314.

[29] D. J. Matic, B. Lovrecek, and D. Skansi. The rotating cylinder electrode. *Journal of Applied Electrochemistry*, 8:391–398, 1978.

[30] Jaeyeong Park, Sungyeol Choi, Sungjune Sohn, and Il Soon Hwang. Cyclic voltammetry on zr, sn, fe, cr and co in LiCl-KCl salts at 500°c for electrorefining of irradiated zircaloy-4 cladding. *Journal of The Electrochemical Society*, 164(12):D744–D751, 2017. doi: 10.1149/2.1501712jes. URL https://doi.org/10.1149/2.1501712jes.

[31] J. C. Poignet and M. J. Barbier. Determination of the diffusion activation coefficients and enthalpies of some cations in the molten licl-kcl eutectic by choronopoteniometry. *Electrochemical Acta*, 17:1227–1233, 1972.

[32] Karthik Ramaswami and J. R. Selman. Rotating disk studies in molten carbonates: II .

meniscus and film effects. *Journal of The Electrochemical Society*, 141(3):622–629, mar 1994. doi: 10.1149/1.2054781. URL https://doi.org/10.1149/1.2054781.

[33] Karthik Ramaswami and J. Robert Selman. Rotating disk studies in molten carbonates: I . electrode design. *Journal of The Electrochemical Society*, 141(3):619–621, mar 1994. doi: 10.1149/1.2054780. URL https://doi.org/10.1149/1.2054780.

[34] Devin Rappleye and Michael F. Simpson. Application of the rotating cylinder electrode in molten licl-kcl eutectic containing uranium(iii)- and magnesium(ii)-chloride. *Journal of Nuclear Materials*, 487:362–372, 2017. ISSN 0022-3115. doi: https://doi.org/10.1016/j.jnucmat.2017.02.037. URL https://www.sciencedirect.com/science/article/pii/S0022311516310480.

[35] Brian J. Riley, Joanna McFarlane, Guillermo D. DelCul, John D. Vienna, Cristian I. Contescu, and Charles W. Forsberg. Molten salt reactor waste and effluent management strategies: A review. *Nuclear Engineering and Design*, 345:94–109, 2019. ISSN 0029-5493. doi: https://doi.org/10.1016/j.nucengdes.2019.02.002. URL https://www.sciencedirect.com/science/article/pii/S002954931930024X.

[36] Nicole Simon, Olivier Gastaldi, Thomas Penit, Olivier Cohin, and Pierre-Yues Campion. On-line reprocessing of a molten salt reactor: A simulation tool. *International Nuclear Information System*, 40(1), 05 2008. URL https://inis.iaea.org/search/search.aspx?orig_q=RN:40003956.

[37] M. M. Tylka, J. L. Willit, J. Prakash, and M. A. Williamson. Application of voltammetry for quantitative analysis of actinides in molten salts. *Journal of The Electrochemical Society*, 162(12):H852–H859, 2015. doi: 10.1149/2.0281512jes. URL https://doi.org/10.1149/2.0281512jes.

[38] Alexander M. Wheeler and Ondřej Chvála. Molten salt reactor sourdough refueling and waste management strategy. *Journal of Nuclear Engineering*, 2(4), 10 2021. ISSN 2673-4362. doi: 10.3390/jne2040033. URL https://www.osti.gov/biblio/1828982.

[39] Tyler Williams, Rankin Shum, and Devin Rappleye. Review—concentration measurements in molten chloride salts using electrochemical methods. *Journal of The Electrochemical Society*, 168(12):123510, dec 2021. doi: 10.1149/1945-7111/ac436a. URL https://doi.org/10.1149/1945-7111/ac436a.

[40] Mark Williamson. Pyroprocessing technologies: Recycling used nuclear fuel for a sustainable future. https://www.ne.anl.gov/pdfs/12_Pyroprocessing_bro_5_12_v14[6].pdf.

[41] Qiufeng Yang, Jianbang Ge, and Jinsuo Zhang. Electrochemical study on the kinetic properties of fe^{2+}/fe, ni^{2+}/ni, cr^{2+}/cr, cr^{3+}/cr^{2+} in molten $mgcl_2 - kcl - nacl$ salts. *Journal of The Electrochemical Society*, 168(1):012504, jan 2021. doi: 10.1149/1945-7111/abdafc. URL https://doi.org/10.1149/1945-7111/abdafc.

[42] Jing Zhang, Jon Fuller, and Qi An. Coordination and thermophysical properties of transition metal chlorocomplexes in licl-kcl eutectic. *The Journal of Physical Chemistry B*, 125:8876–8887, 2021.